Chimeric antigen receptor T cell with an inducible caspase-9 suicide gene eradicates uveal melanoma liver metastases via B7-H3 targeting

Ventin, M.; Cattaneo, G.; Arya, S.; Jia, J.Y.; Gelmi, M.C.; Sun, Y.; ... ; Ferrone, C.R.

Chimeric Antigen Receptor T Cell with an Inducible Caspase-9 Suicide Gene Eradicates Uveal Melanoma Liver Metastases via B7-H3 Targeting

Marco Ventin[1], Giulia Cattaneo[1], Shahrzad Arya[1], Jingyu Jia[1], Maria C. Gelmi[2], Yi Sun[3], Luke Maggs[1], Bruce R. Ksander[4], Robert M. Verdijk[5,6], Genevieve M. Boland[1], Russell W. Jenkins[3,7], Rizwan Haq[7,8], Martine J. Jager[2,4], Xinhui Wang[1], Sandra Ryeom[9], and Cristina R. Ferrone[1,10]

ABSTRACT

Purpose: Uveal melanoma (UM) is the most common intraocular malignant tumor. Despite successful treatment of the primary tumor, about 50% of patients will recur with systemic diseases for which there are no effective treatment strategies. Here we investigated the preclinical efficacy of a chimeric antigen receptor (CAR) T-cell–based immunotherapy targeting B7-H3.

Experimental Design: B7-H3 expression on primary and metastatic human UM samples and cell lines was assessed by RNA sequencing, flow cytometry, and immunohistochemistry. Antitumor activity of CAR T cells targeting B7-H3 was tested *in vitro* with UM cell lines, patient-derived organotypic tumor spheroids from patients with metastatic UM, and in immunodeficient and humanized murine models.

Results: B7-H3 is expressed at high levels in >95% UM tumor cells *in vitro* and *in vivo*. We generated a B7-H3 CAR with an inducible caspase-9 (iCas9) suicide gene controlled by the chemical inducer of dimerization AP1903, which effectively kills UM cells *in vitro* and eradicates UM liver metastases in murine models. Delivery of iCas9.B7-H3 CAR T cells in experimental models of UM liver metastases demonstrates a durable antitumor response, even upon tumor rechallenge or in the presence of a significant metastatic disease burden. We demonstrate effective iCas9.B7-H3 CAR T-cell elimination *in vitro* and *in vivo* in response to AP1903. Our studies demonstrate more effective tumor suppression with iCas9.B7-H3 CAR T cells as compared to a B7-H3-targeted humanized monoclonal antibody.

Conclusions: These studies support a phase I clinical trial with iCas9.B7-H3 CAR T cells to treat patients with metastatic UM.

Introduction

Uveal melanoma (UM) is a rare cancer but is the most common adult ocular malignancy, with an incidence of around six cases per million in the United States (1). At the time of first clinical presentation, about 94% to 96% of patients with UM have localized ocular disease that can be effectively treated with radiotherapy or surgical enucleation. However, despite successful treatment of the primary tumor, approximately 50% of patients with UM will eventually develop metastatic disease primarily in the liver (2). Metastasis is associated with a dismal prognosis, with a 1-year survival rate of 30% and a median overall survival of 4 to 15 months (3). Accordingly, there is an urgent need for more effective treatment of metastatic UM. T-cell–based immunotherapeutic approaches have been at the forefront of recent clinical investigations for treating patients with metastatic UM.

A phase II trial utilizing the adoptive transfer of autologous tumor-infiltrating lymphocytes demonstrated an objective response rate of 35% in patients with metastatic UM (4). More recently, tebentafusp, a bispecific T-cell receptor targeting the gp100/human leukocyte antigen (HLA)-class I complex, demonstrated improved overall survival (from 16.0 to 21.7 months) and disease-free survival (from 2.9 to 3.3 months) in an open-label phase III trial of unresectable metastatic UM (5, 6). However, despite its positive effects on survival outcomes, the HLA-class I dependence of tebentafusp restricts its use to about 45% of patients with UM whose tumors express the HLA-A2-gp100 complex (7). For patients with metastatic UM whose tumors lack the HLA-class I complex, there are no approved targeted or cellular therapy options.

Chimeric antigen receptor (CAR) T-cell therapy has emerged as one of the most promising forms of immunotherapy. CARs are recombinant proteins comprising an extracellular antigen-recognition moiety derived from the single-chain variable fragment of a monoclonal antibody (mAb), linked via a spacer/hinge and transmembrane domain to an intracellular signaling portion with a CD3ζ domain and one or more costimulatory domains (8).

[1]Department of Surgery, Division of Gastrointestinal and Surgical Oncology, Massachusetts General Hospital, Harvard Medical School, Boston, Massachusetts. [2]Department of Ophthalmology, Leiden University Medical Center, Leiden, the Netherlands. [3]Department of Medicine, Mass General Cancer Center, Massachusetts General Hospital, Harvard Medical School, Boston, Massachusetts. [4]Department of Ophthalmology, Schepens Eye Research Institute of Massachusetts Eye and Ear, Harvard Medical School, Boston, Massachusetts. [5]Department of Pathology, Leiden University Medical Center, Leiden, the Netherlands. [6]Department of Pathology, Section Ophtalmic Pathology, Erasmus Medical Center, Rotterdam, the Netherlands. [7]Broad Institute of MIT and Harvard, Cambridge, Massachusetts. [8]Department of Medical Oncology, Dana-Farber Cancer Institute, Harvard Medical School, Boston, Massachusetts. [9]Department of Surgery, Herbert Irving Comprehensive Cancer Center, Columbia University Irving Medical Center, New York, New York. [10]Department of Surgery, Cedars Sinai Medical Center, Los Angeles, California.

M. Ventin and G. Cattaneo contributed equally to this article.

S. Ryeom and C.R. Ferrone are senior authors.

Corresponding Author: Cristina R. Ferrone, Department of Surgery, Cedars-Sinai Medical Center, 8700 Beverly Blvd., Los Angeles, CA 90048. E-mail: cristina.ferrone@cshs.org

Clin Cancer Res 2024;30:3243–58

doi: 10.1158/1078-0432.CCR-24-0071

Translational Relevance

Metastatic uveal melanoma (UM) is a rare cancer and an unmet medical need. The lack of targetable tumor antigens highly and homogeneously expressed has been for decades a major challenge in the field, limiting the development of cellular therapies for the treatment of this highly aggressive tumor. This study identifies B7-H3 as a clinically relevant tumor-associated antigen with a high frequency of expression in UM. We developed a chimeric antigen receptor (CAR) targeting B7-H3 with a newly incorporated inducible caspase-9 (iCas9) suicide gene that demonstrated specific and effective long-term response of UM cells and UM tumors *in vitro* and eradication of established UM liver metastases in mouse models. iCas9.B7-H3 CAR T cells demonstrated more effective metastatic UM tumor eradication as compared to a B7-H3-targeted humanized monoclonal antibody. These results suggest that iCas9.B7-H3 CAR T cells may provide a therapeutic option with significant clinical benefit for patients with metastatic UM.

This approach relies on CAR-redirected T lymphocytes, which allow rapid generation of polyclonal T cells with tumor antigen (TA) specificity and potent HLA class I–independent antitumor activity.

CAR T therapy has revolutionized the treatment of hematological malignancies (9–11) and is being extended to the treatment of solid tumors, with promising clinical trial results (12, 13). In a recent single-arm phase I to II trial of patients with high-risk neuroblastoma, GD2 CAR T cells demonstrated a 65% response rate, with a remarkable 30% of patients achieving a complete response (13). These encouraging results prompted us to investigate whether CAR T-cell therapy could effectively treat metastatic UM. However, successfully developing a CAR T-cell–based strategy for treating patients with metastatic UM requires the identification of a TA expressed at high levels by UM cancer cells. The latter has been a major challenge in the field for the last decades, and a limited number of effective target antigens with variable frequency of expression in UM have been identified (e.g., PRAME, gp100; refs. 14, 15).

B7 homolog 3 (B7-H3), also known as CD276, is a type I transmembrane protein of the B7 ligand family that contains immunomodulatory functions and is associated with disease progression and invasion in several types of cancer (16, 17). B7-H3 is constitutively expressed at high levels across multiple tumor types with restricted expression in normal tissues. Thus, it has been investigated as a potential target for CAR T and antibody-based immunotherapy in solid tumors (18, 19). Single-cell RNA sequencing (RNA-seq) of primary and metastatic UM tumors revealed prognostic significance of the B7-H3 distribution on UM tumor cells (20). However, its pattern and frequency of protein expression are unknown.

Here, we demonstrate that the high expression of B7-H3 in samples from patients with metastatic UM can be targeted *in vitro* and *in vivo* with our novel B7-H3-CAR construct containing an inducible safety switch caspase-9 (iCas9) gene (21). The design of CAR T constructs with a suicide gene-based safety switch allows destruction of the CAR T cells if unexpected toxicities occur (13, 22). Utilizing preclinical mouse models of UM liver metastases we demonstrate the efficacy and durable response of UM tumors to iCas9.B7-H3-targeted CAR T cells. We also aimed to compare our iCas9.B7-H3 CAR T to an anti-B7-H3 monoclonal antibody, currently in clinical trials for the treatment of other solid tumors, in a humanized mouse model of UM liver metastases. Thus, we propose using B7-H3-targeted CAR T-cell therapy as a novel strategy for treating patients with metastatic UM.

Materials and Methods

Study approval

All mouse studies were performed under a protocol (#2013N000014) approved by the Institutional Animal Care and Use Committee (IACUC) at Massachusetts General Hospital.

Study design

The purpose of this study was to investigate the clinical relevance of B7-H3 as a targeted TA in UM and consequently to investigate the preclinical efficacy of B7-H3 CAR T cells *in vitro* and *in vivo*. Furthermore, this study investigated the effective incorporation of an inducible caspase9 safety switch system *in vitro* and *in vivo*. To analyze this approach *in vitro*, we adopted two-dimensional and three-dimensional *in vitro* systems. Animal models of UM liver metastases were established to mimic the clinical course of this disease. The feasibility of this approach was shown in two xenograft models using immunodeficient NSG mice and humanized IL-15 transgenic NSG [NSG-Tg(Hu-IL15)] mice and four different human T-cell donors to demonstrate that the observed effects are independent of the tumor entity and T-cell donors.

Cell lines and culture

The human UM cell lines MP38, MP41, Mel270 and Mel285 derived from primary ocular tumors and OMM2.3 and OMM2.6 derived from liver metastases were kindly provided by Dr. B.R. Ksander (Mass Eye and Ear Research Institute; ref. 23). The UM cell lines MP41, Mel270, and OMM2.3 were transduced with a lentiviral vector-encoding green fluorescent protein (GFP) and luciferase (Luc) and are named MP41-GFP.Luc, Mel270-GFP.Luc, and OMM2.3-GFP.Luc. Viral supernatant was produced by transfection of HEK293T cells with the pMD2.G plasmid (envelope; RRID: Addgene_12259), the psPAX2 plasmid (gag-pol; RRID: Addgene_12260) and the lentiviral vector encoding the GFP.Luc construct (kindly provided by Dr. Joseph Franses, Massachusetts General Hospital). All UM cell lines were cultured in RPMI-1640 culture medium (Corning, catalog #10041CV) supplemented with 10% FBS (Gemini Bio, catalog #900-208) and 2 mmol/L L-glutamine (Thermo Fisher, catalog #25030081) in a humidified 5% CO_2 incubator at 37°C. All UM cells have been authenticated, as described in ref. 23. Jurkat and HEK293T cells were purchased from the American Type Culture Collection (ATCC, RRID: CVCL_0065; RRID: CVCL_0063) and cultured in RPMI-1640 supplemented with 10% FBS. All cell lines were routinely tested for mycoplasma contamination with the MycoAlert Mycoplasma detection kit (Lonza, catalog #LT07-118).

Human data and patient samples

Human UM tissue sample collection

Human tissue collection was performed under a protocol (#11-181) approved by the Institutional Review Board at the Dana-Farber/Harvard Cancer Center and written informed consent was obtained from each subject or each subject's guardian. Formalin-fixed paraffin-embedded tissue samples derived from surgically removed metastatic lesions of patients with UM were kindly provided by the Dr. G.M. Boland BioBank at the Massachusetts General

Hospital (MGH), Dr. R. Haq at the Dana-Farber Cancer Institute. Human tissue samples and clinicopathological data from patients with primary ocular UM tumors were kindly provided by Dr. M. J. Jager at the Leiden University Medical Center. The study was approved by the Scientific Committee of the Ophthalmology Department of the Leiden University Medical Center (project number 29.1). Tumor material was made available for research according to the Dutch FEDERA regulations of leftover material of pathological specimens. The research adhered to Dutch law and the tenets of the Declaration of Helsinki (World Medical Association of Declaration 2013; ethical principles for medical research involving human subjects).

Human UM tissue sample characterization

Chromosome 3 status was determined through single-nucleotide polymorphism with the Affymetrix 250K_NSP-chip and Affymetrix Cytoscan HD chip. Chromosome 8 copy number was obtained by droplet digital polymerase chain reaction and was classified as follows: normal 1.9 to 2.1 copies, gain 2.2 to 3.1 copies, amplification >3.1 copies (24). Follow-up time was calculated as the time from enucleation to death or last follow-up. Tumor pigmentation was scored macroscopically after enucleation on a four-point scale: 1—unpigmented (white), 2—lightly pigmented (gray), 3—moderately pigmented (brown), 4—heavily pigmented (dark brown—black). For the sake of the analysis, groups 1 and 2 were classified as light and groups 3 and 4 were classified as dark. The tumor–node–metastasis stages were classified into two groups: I-IIB and IIIA-IIIC. B7-H3 mRNA expression was measured with the Illumina HT-12v4 chip (Illumina, catalog #BD-901-1001) and was classified as "low" or "high" after splitting the cohort at the median.

The Cancer Genome Atlas cohort and analysis

A retrospective analysis was carried out on The Cancer Genome Atlas (TCGA) database, which contains clinicopathological data of 80 primary UM cases collected in six centers (http://cancergenome.nih.gov/). Information on tumor dimension [largest basal tumor diameter (LBD) and thickness] was determined clinically, while ciliary body involvement was determined through histopathological analysis. Cytological examination was used to identify the cell types in the samples and chromosome status was determined through single nucleotide polymorphism analysis with the ABSOLUTE algorithm. Tumor pigmentation was scored microscopically into three groups: light, mixed, and heavy. More detailed information can be found in Robertson's article (25). mRNA expression of B7-H3 was measured through RNA-seq (Illumina HiSeq 2000, RRID:SCR_020130) and was classified as "low" or "high" after splitting the cohort at the median. For BAP1 status, we classified a case as mutated if a mutation in either RNA-seq or DNA-seq was reported. TCGA groups were classified as follows: A (Disomy 3, normal 8q), B (Disomy 3, 8q gain), C (Monosomy 3, 8q gain), D (Monosomy 3, 8q amplification).

Immunohistochemistry

Fresh human and murine UM specimens were formalin fixed and paraffin embedded by the Histology Research Core Facility at MGH and cut into 4-μm-thick sections and treated according to the standard IHC staining procedure. Briefly, slides were baked overnight, warmed up to 91°C, and treated with CC2 retrieval (NaCit) Ventana 950-223 (catalog #950-223). Then slides were incubated with primary rabbit anti-human B7-H3 mAb (Cell Signaling, RRID:AB_2750877) at a concentration of 5 μg/mL and incubated for 40 minutes at 37°C. Anti-rabbit HRP Ventana 760-4311 (RRID:AB_2811043) was utilized as secondary detection antibody for 60 minutes. The reaction was visualized with DAB chromogen (metastatic UM tumors) or Fast Red (primary ocular UM tumors) substrate 760-159 and bluing reagent 760-2037 were applied as counterstain for 60 minutes. Cover slips were added using histological mounting medium (Fisher, toluene solution, catalog #SP15-100). Stained slides were digitally imaged at 200× objective using the Aperio ScanScope XT (Leica, RRID:SCR_018457). Stained primary UM slides were imaged with a digital slide scanner (Pannoramic 250, 3D Histech, Hungary) and visualized using a slide viewer software (Case Viewer 2.4, 3D Histech, Hungary, RRID:SCR_017654). B7-H3 expression on UM tissue samples was evaluated by a pathologist using an established semiquantitative immunoreactivity score (IRS) approach, as previously described (26) or using the Fiji software (ImageJ, RRID:SCR_002285).

Generation of CAR T cells

Retroviral supernatant preparation

The variable regions of the heavy and light chains of the 376.96 mAb were cloned from the 376.96 mouse hybridoma (27) and then cloned as a single-chain variable fragment into previously validated CAR formats that include the human CD8a hinge and transmembrane domain, CD28 intracellular costimulatory domain, and CD3z intracellular signaling domain. The B7-H3.CAR cassettes were cloned into the retroviral vector SFG. Retroviral supernatants utilized for the transduction of human T cells were produced by transfection of HEK293T cells (ATCC, RRID:CVCL_0063) with the RDF plasmid encoding the RD114 envelope (RRID: Addgene_160604), the PegPam3 plasmid (gag-pol; RRID: Addgene_35614), and the retroviral vector encoding the iCas9.B7-H3-28ζ- CAR, B7-H3-28ζ CAR, or CD19-28ζ CAR construct (kindly provided by Dr. Gianpietro Dotti, University of North Carolina at Chapel Hill, Chapel Hill, NC), as previously described (18).

Transduction and expansion of CAR T cells

Second-generation CAR T cells were generated from unpurified buffy coats obtained from normal human adult donors (Research Blood Components). Peripheral blood mononuclear cells (PBMC) were isolated by density gradient centrifugation (Lymphoprep, STEMCELL, catalog #07851) and plated in a 24-well nontreated tissue culture plate (Thermo Fisher, catalog #142475) precoated with CD3 (1 μg/mL, Miltenyi, catalog #130-093-377) and CD28 (1 μg/mL, BD Bioscience, RRID: AB_396068) antibodies, to induce T-cell activation. Culture medium consisted of equal parts Click's Medium (Irvine Scientific, catalog #9195) and RPMI-1640 (Corning, catalog #10041CV) and are supplemented with 10% FBS (Gemini Bio, catalog #900-208), penicillin (100 U/mL)/streptomycin (100 U/mL; Thermo Fisher, catalog #P433), L-glutamine (2 mmol/L, Thermo Fisher, catalog #25030081), IL-7 (10 ng/mL, Peprotech, catalog #200-07), and IL-15 (5 ng/mL, Peprotech, catalog #200-15). Non-tissue culture–treated 24-well plates were coated overnight with 7 mg/mL retronectin (Takara Bio Inc., catalog #T110A) at 4°C, washed once with 1 mL culture medium, coated with 1 mL/well of retroviral supernatant and centrifuged at 2,000 *g* for 90 minutes. After removal of the supernatant, 4×10^5 activated T cells were plated and centrifuged at 1,000 *g* for 10 minutes. After 72 hours, viral supernatant was removed and replaced with fresh culture medium supplemented with IL-7/IL-15 to allow CAR T-cell expansion.

Natural killer cell isolation and expansion

Human natural killer (NK) cells were isolated from unpurified buffy coats obtained from normal human adult donors (Research Blood Components). PBMCs were isolated by density gradient centrifugation (Lymphoprep, STEMCELL, catalog #07851). Human NK cells were isolated from fresh PBMCs by immunomagnetic negative selection utilizing the EasySep Human NK Cell Isolation Kit (STEMCELL, catalog #19665). Following isolation, NK cells were cultured in RPMI-1640 culture medium (Corning, catalog #10041CV) supplemented with human recombinant IL-2 (500 IU/mL, catalog #200-02) to allow for NK cell expansion.

In vitro co-culture experiments and cytotoxicity assays

3-(4,5-Dimethylthiazol-2-yl)-2,5-diphenyl-2H-tetrazolium bromide assay

Tumor cells were seeded in 96-well tissue culture plates (5,000 cells/well). CAR T cells were added to the culture at effector (CAR T) to target (cancer cells; E:T) ratios of 1:1, 1:4, 1:8, 1:16, 1:32 and incubated at 37°C, 5% CO_2 without the addition of exogenous cytokines. Following a 72-hour incubation, cancer cell viability was assessed by 3-(4,5-dimethylthiazol-2-yl)-2,5-diphenyl-2H-tetrazolium bromide (MTT) assay (Millipore Sigma, catalog #CT02) according to the manufacturer's instructions.

Flow cytometry

UM-GFP.Luc cell lines were seeded in six-well tissue culture plates (50,000 cells/well). CAR T cells were added to the culture at E:T ratio of 1:5 without the addition of exogenous cytokines. Following a 120-hour incubation, residual tumor cells and CAR T cells were harvested and analyzed by flow cytometry. Dead cells were excluded with the Zombie Violet fluorescent live/dead dye (BioLegend, 1:1,000 dilution, catalog #423107). CAR T cells were identified by CD3 expression, while tumor cells were identified by GFP expression. The number of live cancer cells was determined by counting beads (CountBright Absolute Counting Beads, Thermo Fisher, catalog #C36950).

Live-cell imaging

UM-GFP.Luc cell lines were seeded in 96-well tissue culture plates (5,000 cells/well). CAR T cells were stained with the PKH26 Red Fluorescent Cell Membrane Dye (Millipore Sigma, catalog #PKH26GL-1KT) and added to the culture at an E:T ratio of 1:1 without the addition of exogenous cytokines. Tumor cell proliferation was monitored using an Incucyte SX5 Live-Cell Analysis Instrument.

Spheroid preparation and microfluidic culture

Patient-derived organotypic tumor spheroids (PDOTS) were prepared and cultured as previously described (28). Spheroid-collagen mixtures (10 μL) were loaded into the center gel region of a 3D microfluidic culture device (AIM Dax-01, AIM Biotech). Following a 30-minute incubation in sterile humidity chambers at 37°C, collagen hydrogels containing tumor spheroids/PDOTS were hydrated with culture medium (DMEM, CATALOG #11965092, supplemented with 10% FBS, Gemini Bio, catalog #900-208, and 1% penicillin-streptomycin, Thermo Fisher, catalog #P433). CAR T cells were added into the side channel of the culture device at an E:T of 1:1. Viability assessment of PDOTS was performed using dual-label fluorescence-live/dead staining and Hoechst (Thermo Fisher, catalog #H21486)/propidium iodide [Thermo Fisher, catalog #P3566 (Ho/PI)] staining solution, as previously described (28). Images were obtained following incubation with Ho/PI (45 minutes, 37°C, 5% CO_2), and image capture and analysis were performed using a Nikon Eclipse NiE fluorescence microscope equipped with motorized stage (ProScan) and ZYLA4.2 Plus USB3 Camera (Andor) and NIS-Elements AR software package (RRID:SCR_014329). Live and dead cell quantitation was performed by measuring total raw cell area for each dye. Percent change and L2FC data were generated using raw fluorescence data (live) for indicated treatments relative to control conditions.

T-cell proliferation assay

CAR T cells were labeled with 1 mmol/L carboxyfluorescein diacetate succinimidyl ester (CFSE, Invitrogen, catalog #C34554) per the manufacturer's instructions and plated with tumor cells at the E:T ratio of 1:5. Following a 72-hour incubation period CAR T-cell proliferation was measured by flow cytometry based on CFSE dilution on gated CAR T cells.

Effector cytokine profiling assay

Tumor cells were seeded in 24-well tissue culture plates (50,000 cells/well). CAR T cells were added to the culture at the E:T ratio of 1:1 and incubated at 37°C without the addition of exogenous cytokines. Following a 24-hour incubation period, cell culture supernatants were collected and CD8 T/NK cell effector cytokines were measured utilizing a bead-based immunoassay (LEGENDplex V-Bottom Multiplex Assay kit for Human CD8/NK Panel, catalog #741065) per manufacturer's instructions.

Flow cytometry

Expression of B7-H3 on UM cell lines was assessed with the 376.96 mouse anti-human B7-H3-specific mAb clone at a concentration of 1 μg/mL for a 45-minute incubation at 4°C. After washing with PBS containing 0.5% BSA, an allophycocyanin (APC)-conjugated goat anti-mouse secondary antibody (Jackson ImmunoResearch, RRID: AB_2338642) was added (1:100 dilution) for detection. B7-H3 expression was confirmed with an APC-conjugated anti-human CD276 (B7-H3) Ab (BioLegend, clone: MIH42, AB_2564403). The transduction efficiency of CAR T cells was assessed utilizing a FITC-Labeled Human B7-H3 protein (4Ig; Acro Biosystems, catalog #B7B-HF2E7) at the concentration of 2 μg/mL. Flow cytometry was performed utilizing antibodies specific to human CD3 (BD, catalog #612893), CD4 (Cytek, catalog #364-0047-41), CD8 (Bio-Rad, catalog #MCA1226SBB615), CD11b (Bio-Rad, catalog #MCA711SBUV510), CD14 (BioLegend, catalog #301828), CD20 (Bio-Rad, catalog #MCA1710SBY665), CD45 (Bio-Rad, catalog #MCA87GA), CD45RA (Bio-Rad, catalog #MCA88S-BUV510), CD56 (BioLegend, catalog #392435), CD86 (BioLegend, catalog #305441), CCR7 (BD, catalog #569271), PD-1 (BioLegend, catalog #329939), LAG-3 (Miltenyi, catalog #130-125-722), TIM-3 (BD, catalog #570672). All samples were acquired with the Cytek Aurora Flow Cytometry System and results were analyzed utilizing FlowJo v10.9 software (RRID:SCR_008520).

In vivo mouse studies

Mice

Eight-week-old female and male NOD.Cg-Prkdc^{scid} Il2rg^{tm1Wjl}/SzJ (NSG, Strain #005557) mice and 8-week-old male NOD.Cg-*Prkdc*^{scid} *Il2rg*^{tm1Wjl} Tg(IL15)1Sz/SzJ [NSG-Tg(Hu-IL15), Strain #030890] mice were purchased from The Jackson Laboratory. All mice were housed, and experiments were performed in the Animal Facility at MGH. Animal studies were carried out according to the ethical regulations and protocols under the approval of the MGH

IACUC. The power of study and sample size analysis determined that a size of five mice per group will provide >80% power to identify a statistically significant difference by Fisher's exact test at a two-sided 0.05 α level, assuming, based on observed effect estimates, that our treatment will be effective in >80% versus 0% of treated versus untreated mice, respectively.

UM liver metastatic models

MP41-GFP.Luc or OMM2.3-GFP.Luc tumor cells were suspended in 50 uL of PBS and engrafted (5×10^5 cells/mouse) in the spleen of 8-week-old male or female NSG mice. Briefly, mice were anesthetized with ketamine (80–100 mg/kg)/xylazine (5–10 mg/kg) and placed in a right-flank lateral position. The skin was disinfected with a triple saline scrub followed by 70% alcohol, and a 1 cm left subcostal incision was made and the spleen exposed on a 5 × 5 cm sterile gauze. Tumor cells were slowly injected into the ventral hemi-spleen using a 31G sterile syringe. Splenectomy was performed 20 minutes following the injection of UM cells utilizing titanium hemostatic clips (CLIP SLS VITALITEC, Peters Surgical) and a high-temp surgical cautery tip (Argent, McKesson). The wound was closed in two layers with running 5-0 adsorbable polydioxanone suture (Ethicon) and a 9 mm stapler (AutoClips, BRAINTREE SCIENTIFIC, INC.). Twenty or 30 days after tumor cell engraftment, mice were randomized using a simple randomization method and equal distribution was determined using a two-tailed ANOVA test based on total photon flux/second. Following randomization, iCas9.B7-H3-28ζ CAR T cells or CD19-28ζ CAR T cells were injected intravenously (i.v.; 5×10^6 CAR T cells/mouse). Ninety days after CAR T-cell administration, mice were rechallenged by i.v. injection of 5×10^5 MP41-GFP.Luc cells and monitored for 10 weeks. For the iCas9 safety-switch functionality experiment, 20 days after tumor cell engraftment, mice received iCas9.B7-H3-28ζ CAR T cells or B7-H3-28ζ CAR T cells i.v. (5×10^6 CAR T cells/mouse). After 3 and 6 days of CAR T-cell administration, mice received AP1903 (Bellicum) 5 mg/kg or vehicle (corn oil) by intraperitoneal injection.

Humanized xenogeneic UM liver metastatic model

To investigate the antitumor activity of iCas9.B7-H3 CAR T cells and humanized anti-B7-H3 mAb with mUM, 8-week-old male NOD.Cg-*Prkdc*^{scid} *Il2rg*^{tm1Wjl} Tg(IL15)1Sz/SzJ mice [NSG-Tg(Hu-IL15), The Jackson Laboratory, strain# 030890] were grafted in the spleen with MP41-GFP.Luc cells as previously described. Fifteen days after tumor cell engraftment, mice were humanized by tail vein injection of human PBMCs (1×10^7 cells/mouse). For initial validation of the model, 8 days after infusion of PBMCs, blood cell composition was assessed by flow cytometry and counting beads.

Twenty days after tumor cell engraftment, mice received autologous iCas9.B7-H3 CAR T cells (5×10^6 CAR T cells/mouse), humanized anti-B7-H3 IgG1 kappa mAb (enoblituzumab, MedChemExpress, catalog #HY-P9966, 10 mg/kg/mouse) or human IgG1 kappa (MedChemExpress, catalog #HY-P99001, 10 mg/kg/mouse); i.v. enoblituzumab and the human IgG1 kappa isotype control were administered twice weekly for 4 weeks.

In vivo imaging

Bioluminescence imaging

Mice were anesthetized using ~2% isoflurane in oxygen and intraperitoneally injected with D-luciferin Firefly (MedChemExpress, catalog #HY-12591A). Fluorescence intensity was measured by the AMI HTX *in vivo* imaging system (Spectral Instruments Imaging). Image processing and the quantification of photon flux were performed with Aura Imaging software v 4.0.

Magnetic resonance imaging (MRI)

Mice were anesthetized using ~2% isoflurane in oxygen and imaged on a Bruker 4.7 Tesla MRI with a T1 rapid acquisition with relaxation enhancement (RARE) sequence (TE: 13.59 ms, TR: 900 ms, Avg: 8, RARE Factor: 4, Matrix: 256 × 256 × 18, Voxel Size: 0.156 mm × 0.156 mm × 1.0 mm) and a T2 RARE sequence (TE: 60 ms, TR: 4,500 ms, Avg: 6, RARE Factor: 10, Matrix: 256 × 256 × 18, Voxel Size: 0.156 mm × 0.156 mm × 1.0 mm). Images were created in Horos Software v.3.3.6 (horosproject.org, RRID: SCR_017340).

Statistical methods, data analysis, and software

All graphs with error bars report mean ± standard error of mean (SEM) values except where indicated. Statistical tests, number of replicates, and independent experiments are listed in the figure legends. Mann–Whitney U test was used to compare the distribution of B7-H3 expression between categorical variables, and continuous variables were compared using Spearman rho correlation. Disease-specific survival was analyzed with the Kaplan–Meier curve and log-rank test, and patients who died of another or unknown cause were censored. A P value ≤ 0.05 was considered significant. Statistical analysis was performed with SPSS, v. 25 (IBM Corp). GraphPad Prism v. 10 was used for basic statistical analysis and graph plotting (GraphPad, La Jolla, CA, RRID:SCR_002798).

Data availability

The data generated in this study are available upon request from the corresponding author. RNA-seq data were obtained from TCGA PanCancer Atlas Cohort and are publicly available (https://gdc.cancer.gov/about-data/publications/pancanatlas). Requests for usage of the LUMC data can be sent to Dr. Jager (m.j.jager@lumc.nl).

Results

B7-H3 is highly and homogeneously expressed in UM and is associated with more aggressive disease

To investigate the clinical relevance of B7-H3 as a novel target for antibody-based immunotherapy in metastatic UM, we selected a panel of previously described tumor antigens with clinical relevance for CAR T-cell therapy in solid tumors (29) and evaluated their mRNA expression profile among 80 unique UM tumors in TCGA database. After gp100 (*PMEL*), B7-H3 (*CD276*) demonstrated the second highest relative mRNA expression of all TAs analyzed (**Fig. 1A**). Notably, B7-H3 mRNA expression was on average higher than HER2 (*ERBB2*) expression, a tumor target previously considered for CAR T-cell therapy in metastatic UM (30). To confirm the high protein expression of B7-H3, we utilized flow cytometric analyses to assess cell surface B7-H3 expression on primary and metastatic UM cell lines. Our data demonstrate homogeneous and high B7-H3 membrane expression on four UM cell lines (MP38, MP41, Mel270, Mel285) derived from unique primary UM tumors as well as high expression on two metastatic UM cell lines (OMM2.3, OMM2.6) derived from UM liver metastases (**Fig. 1B**). Additionally, high B7-H3 expression (67.1% of positively stained cells) was observed by flow cytometric analysis of a single-cell suspension from a fresh biopsy of a cutaneous UM metastatic lesion (**Fig. 1C**). B7-H3 protein expression was then validated by IHC on unique primary and metastatic UM samples derived from enucleated eye specimens and surgically resected metastatic lesions (**Fig. 1D**). All 43 primary ocular tumors and 18

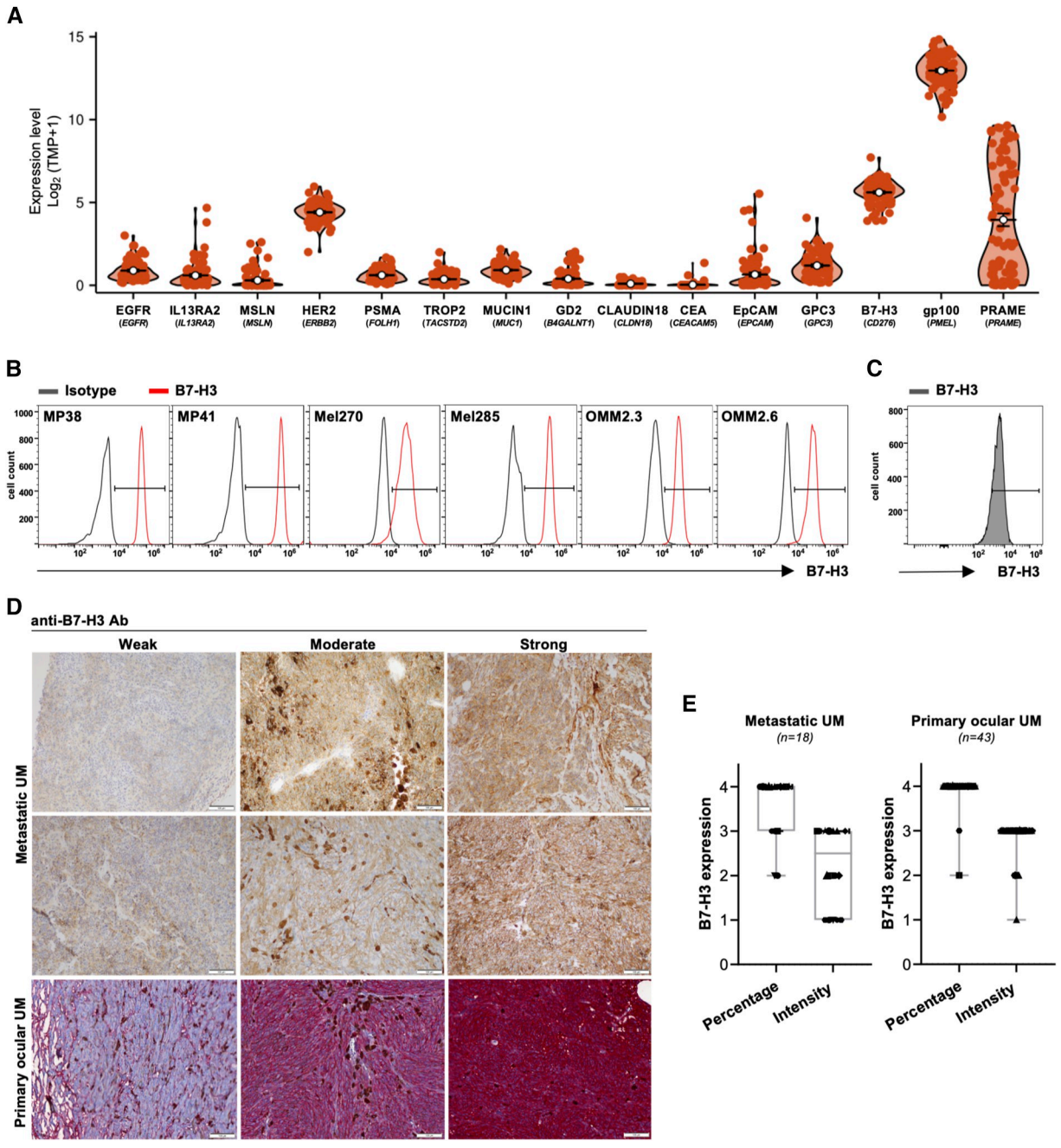

Figure 1.

B7-H3 is highly expressed in primary and metastatic UM. **A,** Violin plot demonstrating mRNA expression levels of 14 genes encoding for tumor antigens with clinical relevance for CAR T-cell therapy in solid tumors ($n = 80$ primary UM tumors, TCGA). **B** and **C,** B7-H3 membrane expression on unpermeabilized UM cell lines (**B**) and a freshly dissociated metastatic UM cutaneous biopsy (**C**) stained with the mouse anti-human B7-H3 mAb 376.96 (1 μg/mL), assessed by flow cytometry. **D,** Representative images of metastatic UM lesions demonstrating weak, moderate, or strong B7-H3 expression by IHC with a rabbit anti-human B7-H3 (5 μg/mL; 200×, scale bar, 100 μm). **E,** Box plots summarizing the frequency and intensity of B7-H3 expression on primary ocular UM tumors ($n = 43$ tumor samples) and metastatic UM lesions ($n = 18$ tumor samples) determined by IRS. Percentage of positively stained cells: 0 < 1%, 1 = 1%–5%, 2 = 6%–25%, 3 = 25%–50%, 4 > 50%; intensity of positively stained cells: 0 = negative, 1 = weak, 2 = moderate, 3 = strong (Created with BioRender.com).

metastatic tumors demonstrated strong B7-H3 membrane expression, as indicated by the IRS assessment (**Fig. 1E**). Of the 61 specimens examined by IHC, 87% ($n = 53/61$) demonstrated 50% to 100% of B7-H3 positively stained cells and only 8.2% ($n = 5/61$) and 4.9% ($n = 3/61$) of samples demonstrated 26% to 50% and 6% to 25% of positively stained cells, respectively. (**Fig. 1E**;

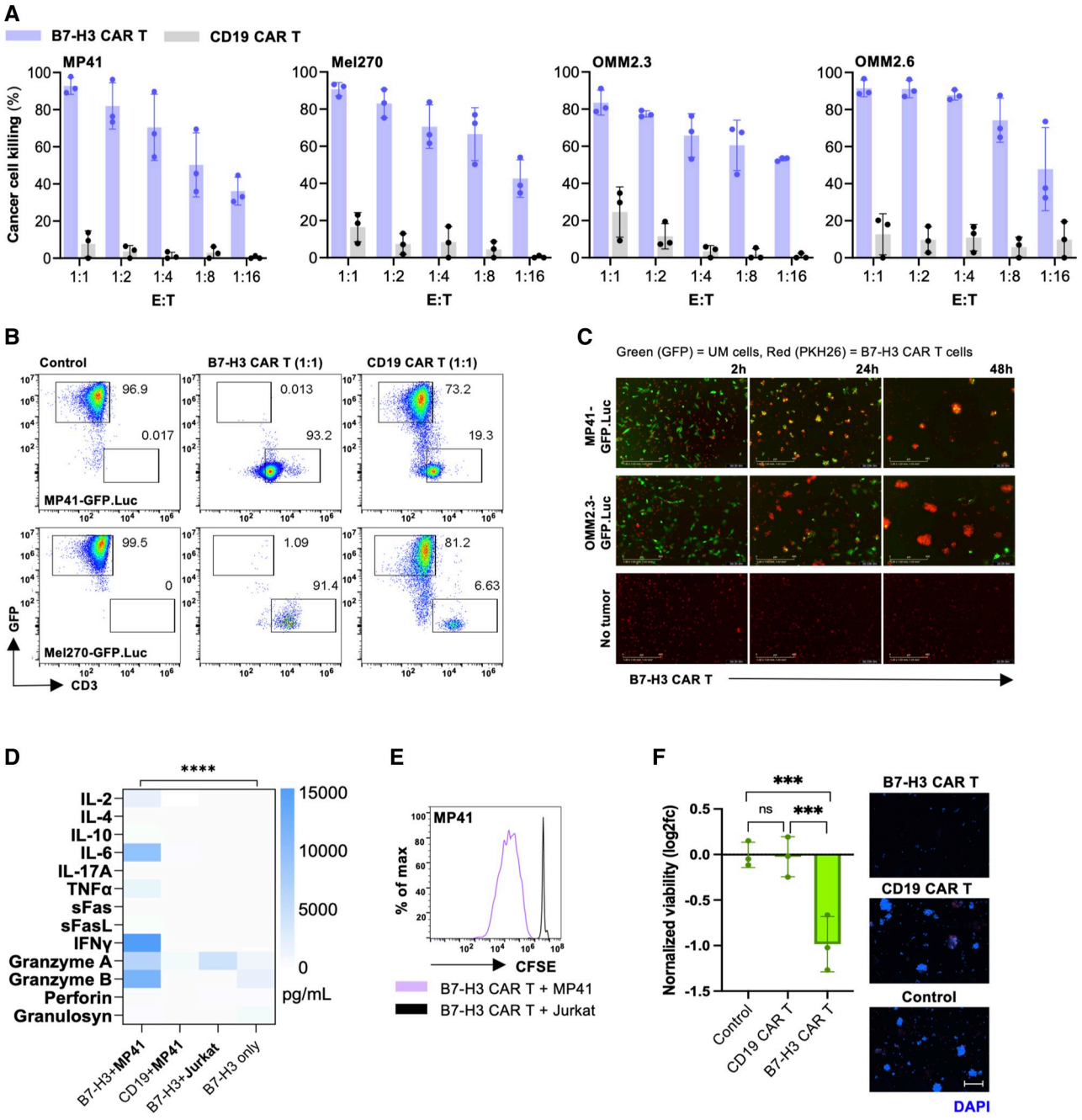

Figure 2.

B7-H3-targeted CAR T cells demonstrate potent *in vitro* antitumor activity with UM cells and patient-derived organotypic metastatic UM spheroids. **A,** Bar plots showing the percentage of UM cell killing mediated by B7-H3 or CD19 CAR T cells at different E:T ratios, assessed by MTT assay after 3 days of co-culture (average of $n = 3$ independent experiments). **B,** Representative flow cytometry plots of residual UM cells after 5 days of co-culture with B7-H3 or CD19 CAR T cells at 1:1 E:T ratio. **C,** Representative images for B7-H3 CAR T-cell (PKH26-red) proliferation and cancer cell (GFP-green) reduction after 2-24-48 hours of co-culture at 1:1 E:T ratio (scale bar, 400 μm). **D,** Summary of effector cytokines released by B7-H3 or CD19 CAR T cells in culture supernatants after 24 hours of co-culture with the indicated cell lines (average of $n = 3$ independent experiments). **E,** Proliferation assay of CFSE-labeled B7-H3 CAR T cells upon co-culture with the indicated cell lines, assessed by flow cytometry. **F,** Bar plots and representative images showing viability of patient-derived organotypic tumor spheroids generated from a UM metastasis after 5 days of co-culture with B7-H3 or CD19 CAR T cells in a 3D microfluidic device ($n = 3$ technical replicates; scale bar, 200 μm). Statistical comparisons were performed using one-way ANOVA with Tukey's multiple comparisons test. ***, P value ≤ 0.001 (Created with BioRender.com).

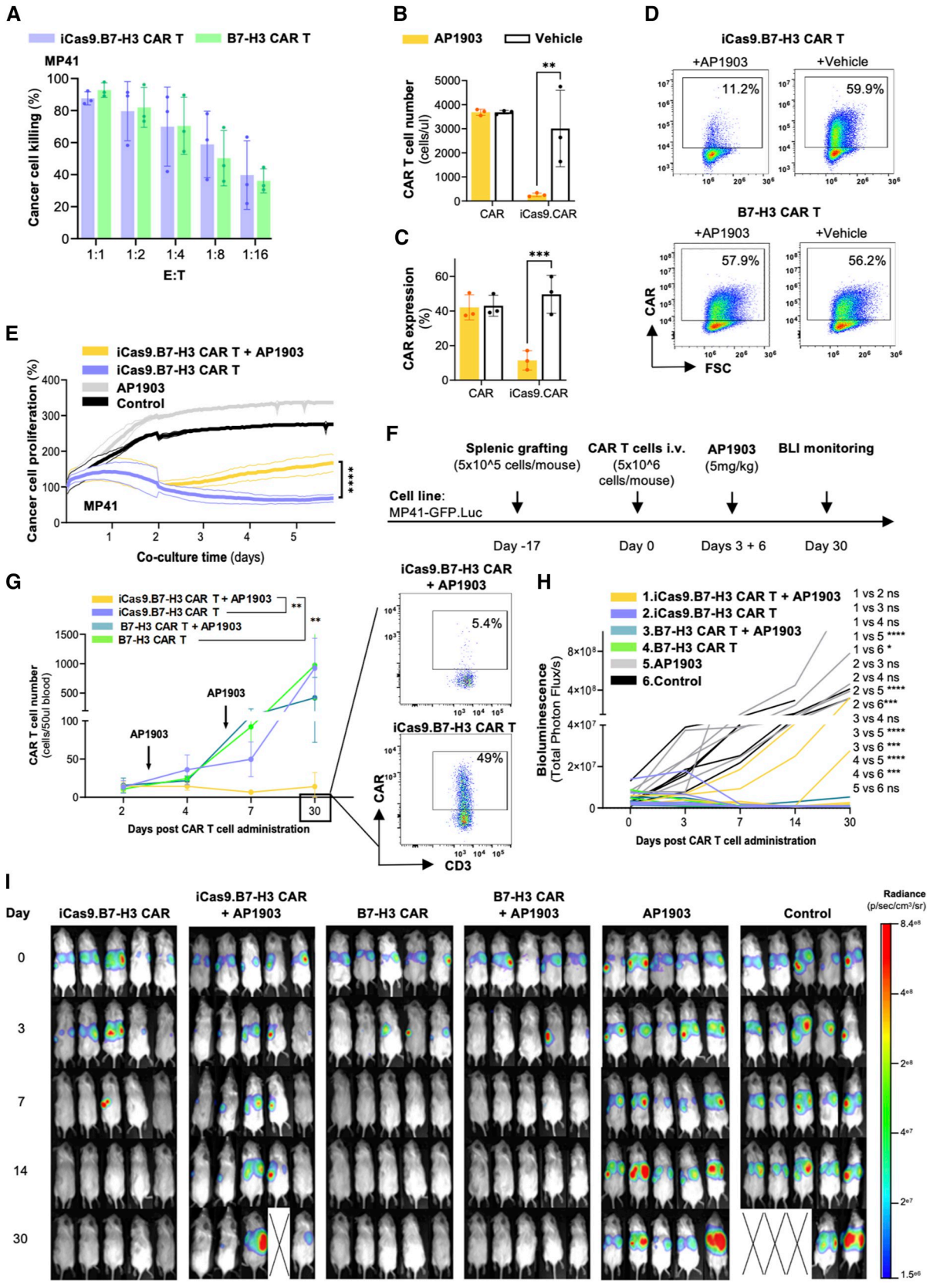

Supplementary Tables S1 and S2). In contrast, B7-H3 expression was not expressed in normal human liver adjacent to UM liver metastasis, as previously shown (Supplementary Table S2; ref. 18). Furthermore, B7-H3 demonstrated homogeneous expression and distribution in patients with multiple lesions, regardless of treatment regimen or status (Supplementary Table S2; ref. 31). In our cohort of 64 primary UM tumors from the Leiden University Medical Center, higher B7-H3 mRNA level was significantly associated with known features of aggressive prometastatic UM tumors, including chromosome 3 monosomy, chromosome 8q gain/amplification, and BAP1 mutation, significantly higher rates of UM liver metastases and reduced survival (Supplementary Table S3; Supplementary Fig. S1A). Our findings were further confirmed on TCGA dataset of 80 primary UM tumors that demonstrated analogous prognostic features and outcomes in relation to B7-H3 mRNA expression level (Supplementary Table S4; Supplementary Fig. S1B). These findings support the validity of B7-H3 as a *bona fide* target antigen for antibody-based immunotherapy in metastatic UM.

B7-H3-targeted CAR T cells show potent *in vitro* antitumor activity against UM

B7-H3-targeted CAR T cells (B7-H3 CAR T), incorporating a CD28 costimulatory domain in the endodomain by retroviral transduction of activated T cells from normal donor PBMCs, were generated. Antitumor activity of B7-H3 CAR T cells against the human UM cell lines MP41, Mel270, OMM2.3, and OMM2.6 was tested. The CD19 CAR T cells were used as a control, as CD19 is not expressed on UM cells. B7-H3 CAR T cells demonstrated complete eradication of UM cells at an effector-to-target (E:T) ratio of 1:1 and a dose-dependent antitumor activity at lower E:T ratios. In contrast, there was minimal killing of UM cells treated with CD19 CAR T cells (**Fig. 2A** and **B**). The antitumor activity of B7-H3 CAR T cells *in vitro* was confirmed by live imaging, which demonstrated rapid and complete eradication of MP41-GFP.Luc UM cells after 48 hours of co-culture (**Fig. 2C**), which persisted for 14 days (Supplementary Fig. S2A). We assessed specific target antigen recognition by measuring the release of effector cytokines by CAR T cells in co-culture supernatants after 24 hours, and CAR T-cell proliferation in response to antigen stimulation. Effector cytokines (IFNγ, TNFα, IL-2, and IL-6), as well as serine proteases (Granzyme A and Granzyme B), were detected in the supernatant when B7-H3 CAR T cells were co-cultured with the MP41 (B7-H3-expressing) cell line, but not with the Jurkat (B7-H3-negative) cell line (**Fig. 2D**). To assess proliferation of B7-H3 CAR T cells in response to antigen stimulation, CFSE-labeled CAR T cells were cultured for 3 days with MP41 cells or Jurkat cells at a 1:1 E:T ratio. B7-H3 CAR T cells proliferated only in co-cultures with MP41 cells but not Jurkat cells (**Fig. 2E**), consistent with the significant production of IFNγ and IL-2. The antitumor activity of B7-H3 CAR T cells was tested with PDOTS from a patient with metastatic UM in 3D microfluidic cultures. Collagen hydrogels containing metastatic UM spheroids were cultured with B7-H3 CAR T cells or CD19 CAR T cells (Supplementary Fig. S2B). B7-H3 CAR T cells but not CD19 CAR T cells infiltrated the collagen matrix and completely eradicated metastatic UM tumor cells over a 96-hour incubation period at an E:T ratio of 1:1 (**Fig. 2F**). Taken together, these results demonstrate target-specific and dose-dependent elimination of B7-H3-expressing UM cells or PDOTS by B7-H3 CAR T cells in 2D and 3D *in vitro* systems.

Rapid elimination of B7-H3 CAR T with an inducible caspase-9 suicide gene

We incorporated an inducible caspase-9-dependent suicide gene (iCas9.B7-H3) in our B7-H3 CAR T construct to control potential CAR T-cell-associated toxicities. As previously demonstrated with CD19 CAR T cells and GD2 CAR T cells, iCas9 enables the safe, prompt, and selective elimination of CAR T cells in preclinical models and patients if CAR T-cell-related toxicities occur (21, 22). Activated T cells from normal donor PBMCs were transduced with either B7-H3 CAR or iCas9.B7-H3 CAR vectors (Supplementary Fig. S3A) with 80% transduction efficiency of both vectors (B7-H3 CAR: 80% ± 4% and iCas9.B7-H3 CAR: 80% ± 5%, $P = 0.936$; Supplementary Fig. S3B). Incorporation of the iCas9 gene did not alter the B7-H3 CAR T-cell effector function, as demonstrated when B7-H3 CAR T cells and iCas9.B7-H3 CAR T cells were co-cultured with MP41 cells. No significant difference was observed in their antitumor activity, which resulted in the complete eradication of MP41 cells at an E:T of 1:1 and with comparable antitumor activity at lower E:T ratios (**Fig. 3A**). Cell culture supernatants collected after 24 hours of co-culture demonstrated comparable release of CAR T-cell activation markers and effector cytokines (IL-2, IL-6, IFNγ, TNFα, Granzyme B and perforin; Supplementary Fig. S3C), which was consistent with their effector activity against UM cells (**Fig. 3A**). Administration of a chemical inducer of dimerization (AP1903) demonstrated rapid and selective *in vitro* elimination of iCas9.B7-H3 CAR T cells (**Fig. 3B–D**). Administration of AP1903 dimerizes and activates caspase-9, which in turn activates downstream caspases, leading to T-cell apoptosis within 6 hours (**Fig. 3B** and **C**). The functional effect of the iCas9-based safety switch was further confirmed by the expansion of both MP41 and OMM2.3 UM cells after AP1903 administration with iCas9.B7-H3 CAR T (**Fig. 3E**; Supplementary Fig. S3D).

To evaluate the antitumor activity of iCas9.B7-H3 CAR T cells and the safety-switch functionality *in vivo*, we generated an

Figure 3.

In vitro and *in vivo* functionality of the iCas9-based safety switch with B7-H3 CAR T cells. **A,** Bar plots showing percentage of UM cell killing mediated by iCas9.B7-H3 or B7-H3 CAR T cells at different E:T ratios, assessed by MTT assay after 3 days of co-culture ($n = 3$ independent experiments). **B** and **C,** Bar plots showing iCas9.B7-H3 or B7-H3 CAR T absolute cell counts and percentage of CAR expression after 6 hours of incubation with AP1903 (10 nm) or vehicle, assessed by flow cytometry ($n = 3$ independent experiments). **D,** Representative flow cytometry plots of iCas9.B7-H3 CAR expression after 6 hours of incubation with AP1903 (10 nm) or vehicle. **E,** Live monitoring of MP41 UM cell growth co-cultured with iCas9.B7-H3 CAR T cells following administration of AP1903 (10 nmol/L). **F,** Schema of metastatic UM xenograft model (MP41.GFP-Luc) infused with CAR T cells. **G,** CAR T-cell ($CD3^+CD45^+$) expansion and response to AP1903 in peripheral blood (50 μL) of mice bearing MP41-derived UM liver metastases ($n = 5$ mice/group). **H,** Total photon flux as a function of time after initiation of CAR T-cell treatment ($n = 5$ mice/group). **I,** Metastatic UM tumor burden measured by BLI in each group treated as indicated ($n = 5$ mice/group), (X denotes mice dead of disease). Statistical comparisons were performed using two-way ANOVA with Sidak's multiple comparisons test (**A–C**), Tukey's multiple comparisons test (**G** and **H**), and Wilcoxon rank-sum test (**E**). *, P value ≤ 0.05; **, P value ≤ 0.01; ***, P value ≤ 0.001; ****, P value ≤ 0.0001 (Created with BioRender.com).

experimental liver metastatic UM model by grafting GFP and luciferase transduced MP41 (MP41-GFP.Luc) cells in the spleen of NOD/SCID/gamma(c; null; NSG) mice (**Fig. 3F**). After the presence of UM liver metastases was confirmed by bioluminescence imaging (BLI) on day 17, mice were randomized to the treatment groups. iCas9.B7-H3 CAR T or B7-H3 CAR T cells were administered via tail vein injection. CAR T cells generated with each CAR construct demonstrated similar *in vivo* expansion (**Fig. 3G**), which resulted in complete eradication of UM liver metastases 7 days after either iCas9.B7-H3 CAR T or B7-H3 CAR T-cell administration (**Fig. 3H** and **I**). The *in vivo* functionality of the safety switch was demonstrated by the selective and rapid elimination of circulating iCas9.B7-H3 CAR T cells upon AP1903 administration at both 3 and 6 days after CAR T-cell injection (**Fig. 3F**; Supplementary Fig. S3E) and no detection of circulating IFNγ or perforin on day 4 after AP1903 administration (Supplementary Fig. S3F). Despite AP1903-mediated destruction of circulating iCas9.B7-H3 CAR T cells 7 days after CAR T delivery (Supplementary Fig. S3G), two out of five mice still achieved a near complete response following CAR T-cell administration after only 3 days of iCas9.B7-H3 CAR treatment that persisted up to 30 days (**Fig. 3I**). Of them, one mouse had few circulating CAR T cells (10 CAR T/50 uL blood), and one mouse had a slightly higher number (27 CAR T/50 uL blood) of circulating iCas9.B7-H3 CAR T cells, which could have contributed to sustained tumor control. The mean number of CAR T cells/50 uL of blood in the iCas9.B7-H3 CAR T + AP1903 group [11.0 (SD ± 11.3)] was, however, significantly lower compared to the group that did not receive AP1903 [923.9 (SD ± 508.4), $P = 0.015$; Supplementary Fig. S3G].

iCas9.B7-H3 CAR T cells demonstrate sustained antitumor activity against UM liver metastases and tumor rechallenge

We next investigated the long-term *in vivo* antitumor activity of iCas9.B7-H3 CAR T cells by generating a liver metastatic UM model utilizing OMM2.3 cells established from a UM liver metastasis, that was transduced with GFP and luciferase (OMM2.3-GFP.Luc; **Fig. 4A**). iCas9.B7-H3 CAR T cells achieved complete tumor eradication and demonstrated sustained antitumor activity by doubling the survival of mice monitored for up to 90 days, compared to the untreated group or mice treated with the control CD19 CAR T cells (**Fig. 4B** and **C**). Circulating iCas9.B7-H3 CAR T cells were detected in peripheral blood 90 days after CAR T-cell administration (Supplementary Fig. S3H).

We next validated the long-term antitumor activity of iCas9.B7-H3 CAR T cells and investigated the ability of persistent circulating iCas9.B7-H3 CAR T cells to mount an antitumor response, by utilizing a second UM cell line derived from a primary ocular tumor. NSG mice grafted with MP41-GFP.Luc cells (**Fig. 4D**) were treated with iCas9.B7-H3 CAR T cells and monitored for metastatic UM tumors by BLI for up to 87 days (**Fig. 4E–G**). Mice were then rechallenged with MP41-GFP.Luc cells via tail vein injection and monitored for tumor growth. After 172 days, all mice from the iCas9.B7-H3 CAR T group were still alive, with 2/5 mice demonstrating sustained tumor rejection and 3/5 mice demonstrating partial responses after tumor rechallenge, compared to untreated controls, which were euthanized due to excessive tumor burden on days 120 and 150 (**Fig. 4E–G**). Prior to the tumor rechallenge (on day 86), circulating iCas9.B7-H3 CAR T cells were detected in all mice. In contrast, 5 days after tumor rechallenge, we observed a significant increase in circulating CAR T cells. Tumor eradication appears to correlate with iCas9.B7-H3 CAR T expansion as two mice with the most robust anti-tumor response had the highest levels of circulating CAR T cells (**Fig. 4H**) and notably high levels of subpopulations of $CCR7^+CD45RA^+$ T memory stem cells (T_{SCM}; **Fig. 4I**). When mice were sacrificed at the end of experiment, T cells were still detectable in peripheral blood and bone marrow (**Fig. 4J** and **K**).

iCas9.B7-H3 CAR T cells demonstrate complete pathological response in mice with high metastatic burden

Recent clinical studies reported that high tumor burden correlates with poor response to CAR T-cell therapy in hematological malignancies because of the unfavorable E:T ratio, and the inability of a tumor-burdened immune system to mount an effective immune response to overcome extensive tumor load (32–34). Thus, we examined the ability of our iCas9.B7-H3 CAR T to eradicate significant metastatic disease. Mouse models with a high and low hepatic UM tumor burden were established by grafting MP41-GFP.Luc cells in the spleen of NSG mice on day −25 (high tumor burden) and day −17 (low tumor burden; **Fig. 5A**). Once the presence of high and low tumor burden UM liver metastases was confirmed by BLI (**Fig. 5B**), iCas9.B7-H3 CAR T cells were administered by tail vein injection. MRI was utilized to monitor the objective clinical response up to 30 days. Thirty days after CAR T-cell administration, iCas9.B7-H3 CAR T cells induced a complete clinical (**Fig. 5C**) and pathological (Supplementary Fig. S4A) response in mice harboring low tumor burden UM liver metastases and also induced complete regression of extensive macroscopic disease in the liver (**Fig. 5C**; Supplementary Fig. S4B). Liver weights of treated mice from the high tumor burden group were significantly lower than untreated controls and were similar to the low tumor burden group (**Fig. 5D**). These findings were confirmed both macroscopically and by IHC (Supplementary Fig. S4A and S4B). On day 10 after CAR T-cell administration, peak CAR T-cell expansion (**Fig. 5E** and **F**), activation (IFN-γ), and secretion of cytotoxic effector molecules Granzyme B, granulysin and perforin (**Fig. 5G**) was observed, which was consistent with significant regression of liver metastases on MRI. Despite this marked CAR T-cell expansion, an increase in the expression of markers associated with T-cell exhaustion (PD-1, TIM-3, LAG-3) at 10, 20, and 30 days after CAR T-cell administration was not observed (**Fig. 5H**). Lastly, although iCas9.B7-H3 CAR T cells induced significant clearance of extensive metastatic burden, few residual lesions demonstrated significantly decreased B7-H3 intensity of staining (Supplementary Fig. S4B and S4C), raising the possibility of TA downregulation as a mechanism of resistance to complete tumor eradication (35).

iCas9.B7-H3 CAR T cells are more effective than B7-H3-targeted humanized monoclonal antibody in humanized mice

Since B7-H3 has been successfully targeted by antibody-based immunotherapy in other solid tumors, we assessed the efficacy of the humanized anti-B7-H3 monoclonal antibody (mAb) against UM cells *in vitro* and compared it to the iCas9.B7-H3 CAR T in humanized mice (Supplementary Fig. S5) with UM liver metastases. We first co-cultured UM cells (MP41, OMM2.3) with freshly isolated NK cells from normal human donors ($n = 3$ independent donors) in the presence of the humanized anti-B7-H3 mAb or an IgG1k isotype control. We observed intrinsic cytotoxic activity mediated by NK cells, which may be attributed to the interaction between NKG2D receptor on NK cells and its ligands (ULBPs, MICA/B), usually overexpressed on cancer cells (**Fig. 6A**; ref. 36). Growth inhibition of MP41 and OMM2.3 target cells by antibody-

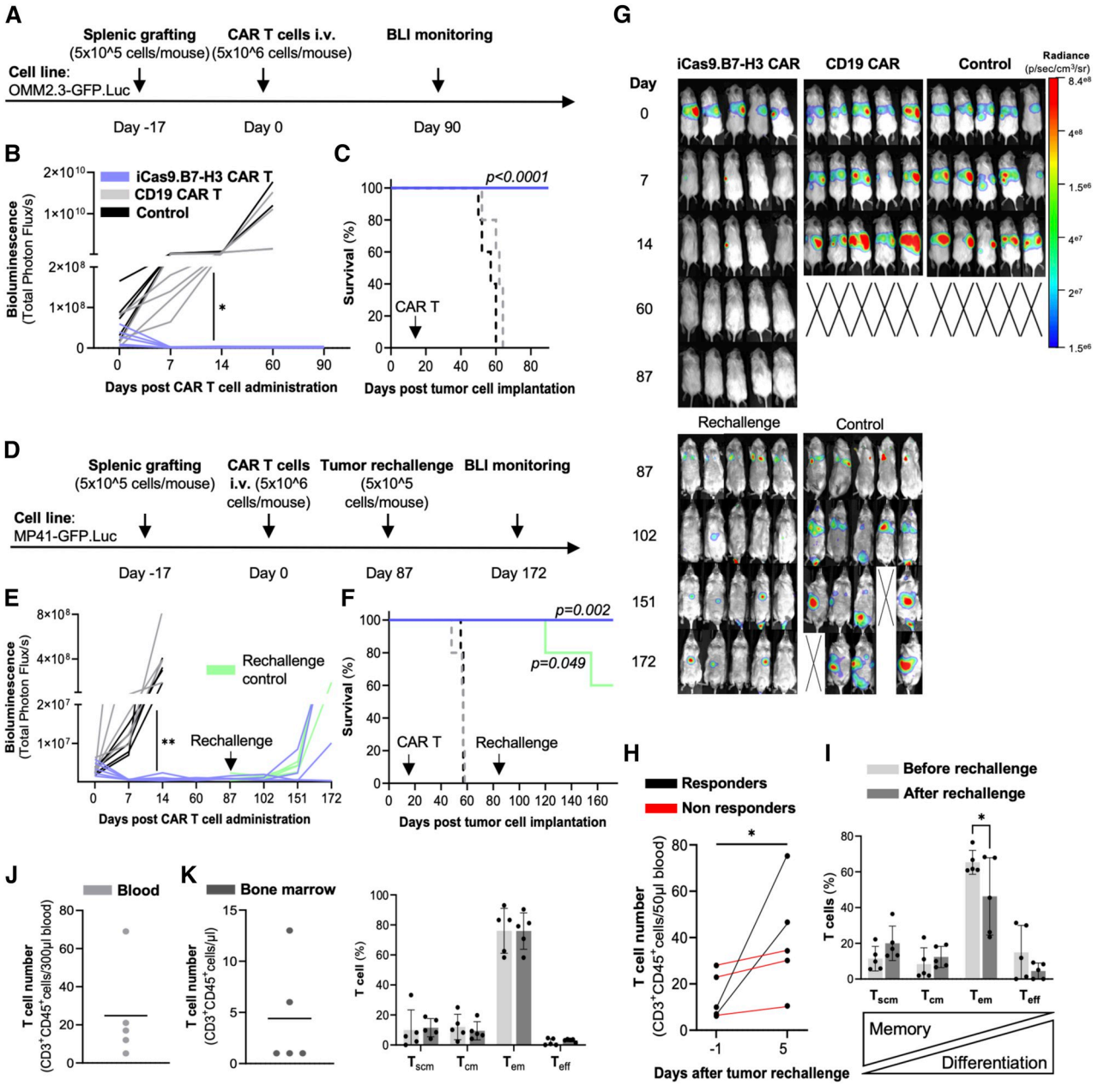

Figure 4.

iCas9.B7-H3 CAR T cells mediate sustained antitumor activity against UM liver metastases and response to tumor rechallenge (**Fig. 3**). *In vitro* and *in vivo* functionality of the iCas9-based safety switch with B7-H3 CAR T cells. **A,** Schema of metastatic UM xenograft model (OMM2.3.GFP-Luc) infused with CAR T cells. **B,** Total photon flux as a function of time after initiation of CAR T-cell treatment ($n = 5$ mice/group). **C,** Kaplan–Meier survival curve of mice ($n = 5$ mice/group). **D,** Schema of metastatic UM xenograft model (MP41.GFP-Luc) infused with CAR T cells and rechallenged with MP41.GFP-Luc cells by tail vein injection. **E,** Total photon flux as a function of time after initiation of CAR T-cell treatment and tumor rechallenge ($n = 5$ mice/group). **F,** Kaplan–Meier survival curve of mice bearing UM tumors in each group after tumor rechallenge ($n = 5$ mice/group). **G,** Metastatic UM tumor burden measured by BLI in each group treated as indicated ($n = 5$ mice/group), (X denotes mice dead of disease). T-cell ($CD3^+CD45^+$; **H**) count and (**I**) phenotype in peripheral blood of mice ($n = 5$ biological replicates) assessed by flow cytometry before and after tumor rechallenge. T-cell (**J**) count and (**K**) phenotype in peripheral blood and bone marrow of mice ($n = 5$ biological replicates) assessed by flow cytometry at the time of sacrifice. Statistical comparisons were performed using two-way ANOVA with Tukey's multiple comparisons test (**B** and **E**), Sidak's multiple comparisons test (**I** and **K**), log-rank test (**C** and **F**), and Mann–Whitney *t* test (**H**). *, *P* value ≤ 0.05; **, *P* value ≤ 0.01; ***, *P* value ≤ 0.001; ****, *P* value ≤ 0.0001 (Created with BioRender.com).

dependent cellular cytotoxicity (ADCC) was significantly higher when NK cells and UM cells were co-cultured in the presence of the anti-B7-H3 mAb, which was consistent with a significant release of effector cytokines (IFNγ, TNFα, IL-6), effector proteins (Perforin) and proteases (Granzyme A, Granzyme B), detected in the supernatant collected 24 hours after co-culture (**Fig. 6A** and **B**). Utilizing

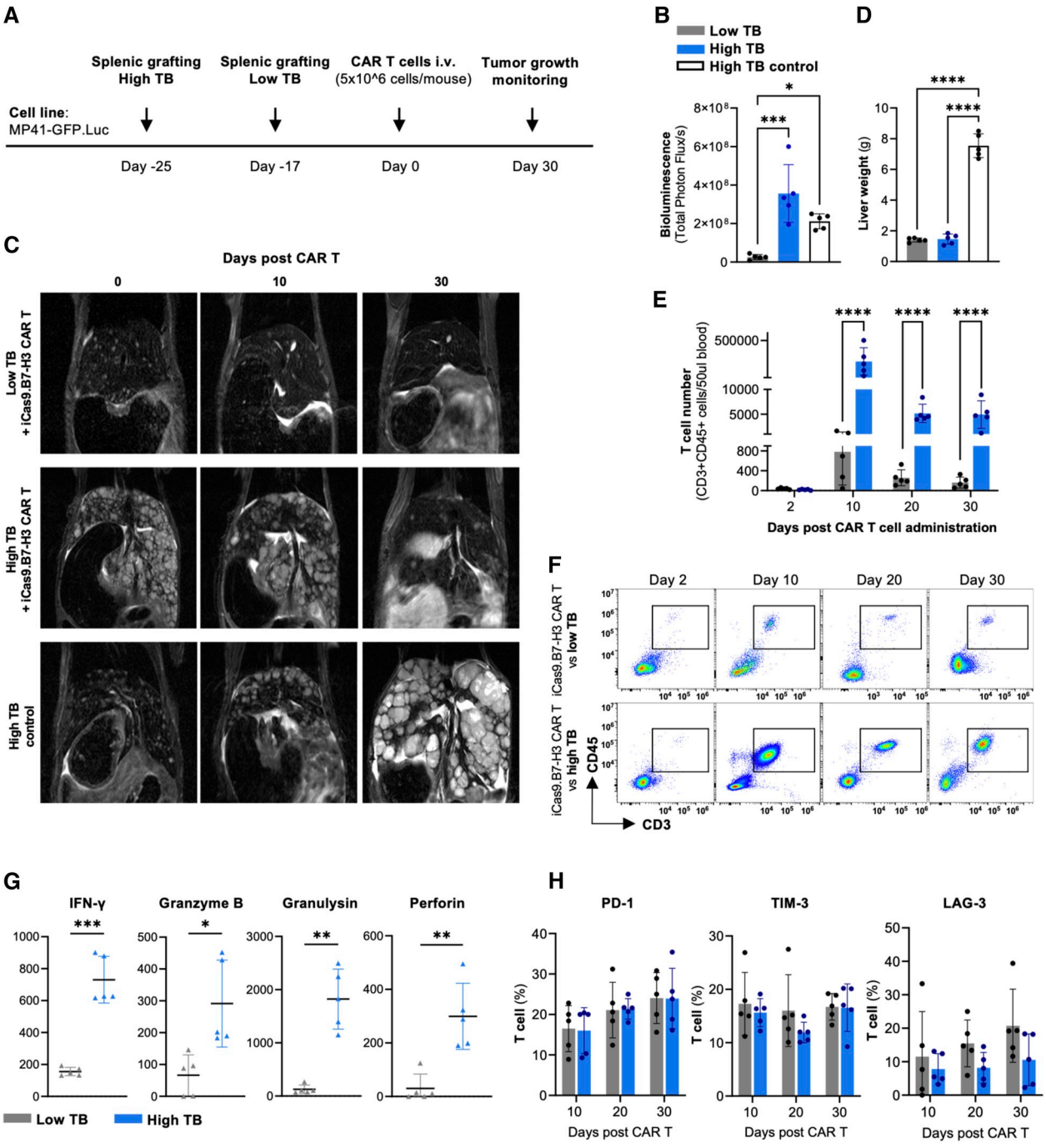

Figure 5.

iCas9.B7-H3 CAR T cells demonstrate the complete and objective pathological response to low and high tumor burden UM liver metastases. **A,** Schema of metastatic UM xenograft model (MP41.GFP-Luc) infused with CAR T cells. **B,** Baseline total photon flux/s at the time of CAR T-cell treatment administration (n = 5 mice/group). **C,** Representative consecutive MRI scans of high and low tumor burden UM liver metastasis response to CAR T-cell treatment. **D,** Bar plots representing the liver weight of mice from described groups sacrificed after 30 days of treatment (n = 5 mice/group). **E,** T-cell ($CD3^+CD45^+$) count in peripheral blood (50 μL) of high and low tumor burden–bearing mice assessed by flow cytometry (n = 5 mice/group). **F,** Representative dot plots of T-cell expansion in high and low tumor burden bearing mice. **G,** Effector cytokine and cytotoxic molecule levels were detected in mice serum on day 10 after CAR T infusion (n = 5 biological replicates/group). **H,** Frequency of iCas9.B7-H3 CAR T cells expressing markers associated with T-cell exhaustion ($CD3^+PD\text{-}1^+$, $CD3^+TIM3^+$ or $CD3^+LAG3^+$, in peripheral blood collected from treated mice 10, 20, and 30 days post CAR T injection (n = 5 biological replicates/group). Statistical comparisons were performed using one-way ANOVA with Tukey's multiple comparisons test (**B** and **D**), two-way ANOVA with Sidak's multiple comparisons test (**E** and **H**), unpaired t test (**G**). *, P value ≤ 0.05; **, P value ≤ 0.01; ***, P value ≤ 0.001; ****, P value ≤ 0.0001 (Created with BioRender.com).

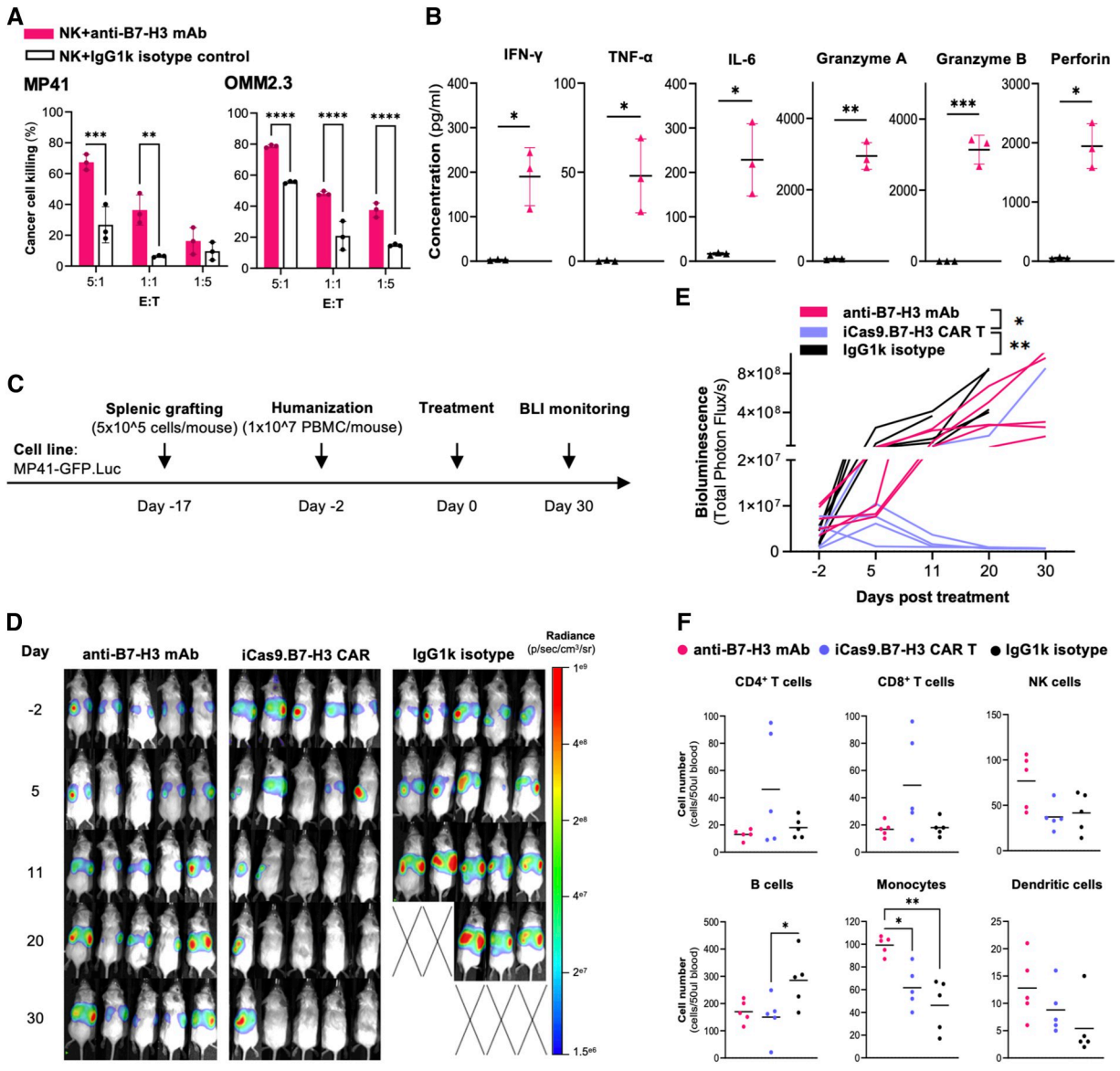

Figure 6.

iCas9.B7-H3 CAR T cells demonstrate more effective suppression of tumor growth than a B7-H3-targeted humanized monoclonal antibody in humanized mice. **A,** Bar plots showing percentage of UM cell killing mediated by freshly isolated NK cells from normal donor PBMCs at different E:T ratios, assessed by MTT assay after 24 hours of co-culture in the presence of anti-B7-H3 mAb or IgG1k isotype control (both at the concentration of 10 mg/mL; $n = 3$ independent experiments). **B,** Effector cytokine and cytotoxic molecule levels released by NK cells in culture supernatants after 24 hours of co-culture with the indicated cell lines in the presence of anti-B7-H3 mAb or IgG1k isotype control (both at the concentration of 10 mg/mL; $n = 3$ independent experiments). **C,** Schema of humanized metastatic UM xenograft model (MP41.GFP-Luc). **D,** Metastatic UM tumor burden measured by BLI in each group treated as indicated ($n = 5$ mice/group). **E,** Total photon flux as a function of time after treatment initiation ($n = 5$ mice/group). **F,** Characterization of circulating immune cells [$CD3^+CD4^+$ ($CD4^+$T), $CD3^+CD8^+$ ($CD8^+$T), $CD56^+$ (NK), $CD20^+$ (B). $CD11c^+$ (monocytes), $CD11c^+CD86^+$ (dendritic cells)] assessed by flow cytometry on day 7 after treatment initiation. Statistical comparisons were performed using two-way ANOVA with Sidak's multiple comparisons test (**A**), Tukey's multiple comparisons test (**E**), one-way ANOVA with Tukey's multiple comparisons test (**F**), and unpaired *t* test (**B**). *, *P* value ≤ 0.05; **, *P* value ≤ 0.01; ***, *P* value ≤ 0.001; ****, *P* value ≤ 0.0001 (Created with BioRender.com).

a humanized murine model, we grafted MP41-GFP.Luc cells in NSG-Tg(Hu-IL15) mice (**Fig. 6C**; Supplementary Fig. S5A), which allows sustained T- and NK-cell expansion through endogenous production of human IL-15. Two days following the humanization process with human normal donor-derived PBMCs, mice were treated with an anti-B7-H3 mAb or IgG1k isotype control for 4 weeks. Simultaneously, a cohort of mice received autologous iCas9.B7-H3 CAR T cells. iCas9.B7-H3 CAR T cells eradicated UM liver metastases in 4/5 mice after 30 days. In comparison, mice treated with the anti-B7-H3 mAb demonstrated a partial response with all mice exhibiting residual tumor after 30 days (**Fig. 6D** and **E**). Flow cytometric analysis of circulating immune cells in our

cohorts after 7 days of treatment demonstrates expansion of NK cells and monocytes, specifically in anti-B7-H3 mAb-treated mice (**Fig. 6F**). These data support the use of iCas9.B7-H3 CAR T cells for the treatment of UM liver metastasis.

Discussion

Limited treatment options are available to patients. B7 homolog 3 (B7-H3), also known as CD276, is a type I transmembrane protein of the B7-ligand family that contains immunomodulatory functions and is associated with disease progression and invasion in metastatic UM. In this study, we investigated the clinical relevance of B7-H3 as a targeted-TA in UM and the preclinical efficacy of B7-H3-targeted CAR T-cell immunotherapy to treat metastatic UM. We found that B7-H3 is expressed in 100% of primary and metastatic UM tumors that we examined. B7-H3-targeted CAR T cells with an inducible caspase9 (iCas9)-based safety-switch induced an effective and sustained antitumor response against UM liver metastases in immunodeficient mouse xenograft models even after tumor rechallenge or in the presence of significant metastatic disease burden. Lastly, in a humanized mouse model of UM liver metastases, we demonstrated that iCas9.B7-H3 CAR T cells were more effective than a humanized anti-B7-H3 monoclonal antibody (mAb) in clinical trials for other solid tumors.

Low tumor immunogenicity has been a major challenge in the field of UM with limited responses to different immunotherapeutic strategies, such as immune checkpoint inhibitors and adoptive T-cell transfer (2, 37). This hurdle has been partially overcome with tebentafusp, a soluble affinity-enhanced HLA-A*02:01–restricted T-cell receptor specific for the glycoprotein 100 (gp100) peptide, which demonstrated survival benefit in patients with metastatic UM and was the first FDA approved therapy specifically for metastatic UM (5). However, the use of tebentafusp is restricted to about 45% of UM patients expressing the targeted HLA-class I/gp100 complex (7). These inherent limitations in the treatment of UM prompted a long investigation for effective TAs constitutively expressed in UM as targets for mAb-based immunotherapeutic approaches. Our data demonstrate that B7-H3 is ubiquitously expressed at high levels in all primary (43/43) and metastatic (19/19) surgically resected UM tumors or biopsies, and human UM cell lines (6/6) with restricted expression on normal tissues, supporting B7-H3 as a clinically relevant target for CAR T-cell immunotherapy in UM. Remarkably, the frequency of B7-H3 expression in UM appears to be higher than in other solid tumors, with studies demonstrating B7-H3 overexpression in 60% to 70% of patients (16, 18). Current options for second line treatment in metastatic UM are primarily investigational compounds. Our data suggest that B7-H3 immunotargeting is a promising avenue for clinical investigation in metastatic UM, as it could be applied to most, if not all patients, overcoming restrictions associated with currently available treatment options. Most importantly, previous and ongoing clinical trials have demonstrated safety and efficacy of B7-H3 immunotargeting in different solid tumors, further supporting B7-H3 as a *bona fide* TA target (16).

Based on these findings, we developed a CAR T cell-based strategy by generating a B7-H3 CAR construct derived from the B7-H3-specific 376.96 mAb (27). We have previously demonstrated significant preclinical antitumor activity of B7-H3 CAR T cells with multiple types of solid tumors, some of which are currently under clinical investigation (NCT04670068, NCT05366179; refs. 18, 38–40). This study demonstrates that B7-H3-directed CAR T cells represent a highly effective therapeutic strategy for metastatic UM. B7-H3 CAR T cells induced complete eradication of UM cells *in vitro*, even at low E:T ratios, which has clinical relevance for CAR T use in treating solid tumors (32, 40, 41). In several preclinical studies, CAR T cells targeting different tumors and TAs achieved complete eradication of solid tumor cells only at high E:T ratios of 20:1 or 10:1, with *in vivo* studies in mouse models demonstrating a cytostatic effect but not complete eradication of solid tumors, suggesting variable tumor cell sensitivity to CAR T-cell effector function (42, 43). Forsberg and colleagues (30), using HER2-targeted CAR T cells, required a 3:1 E:T to induce complete/near-complete eradication of MEL202 and 92-1 UM cells over 48 hours of co-culture. Although variabilities in CAR design must be considered (CAR transduction efficiency, co-stimulatory domain), our findings demonstrate the high sensitivity of UM cells to B7-H3-targeted CAR T cells. These findings were further confirmed *in vivo* using xenograft mouse models of UM liver metastases. The use of mouse models of UM liver metastases we propose is clinically relevant, as the vast majority of patients with UM who recur after successful treatment of the primary ocular tumor recur in the liver (3). At the time of clinical investigation, most patients with UM will likely present with advanced metastatic tumor burden, which could represent a major limitation for successful response to CAR T-cell therapy and higher risk of CAR T-cell–related toxicities (34, 44). Despite these inherent limitations, we have observed B7-H3 CAR T-cell–mediated objective pathological response and eradication of extensive UM liver metastases, which may further support the high susceptibility of UM tumors to B7-H3 targeting and CAR T cells as an effector mechanism.

One concern with the therapeutic use of CAR T cells is related to the well-documented life-threatening toxicities that can occur in patients due to both CAR T-cell expansion and release of cytokines (IL-1, IL-6) triggering immune effector cell–associated neurotoxicity syndrome (ICANS) and cytokine release syndrome (CRS; ref. 45). To alleviate these concerns, we generated a CAR T construct with a highly effective inducible caspase-9 (iCas9)-based "safety-switch," which allows rapid and selective elimination of CAR T cells should CRS or ICANS occur and do not respond to the current standard of care interventions such as steroids and IL-1 and IL-6 inhibitor. Administration of AP1903 dimerizes and activates caspase-9, which activates downstream caspases, leading to T-cell apoptosis within less than 24 hours. This strategy led to abrupt improvement of steroid-refractory ICANS occurring after CD19-specific CAR T cells and the elimination of 90% of CAR T cells from circulation within 24 hours (22). Importantly, we demonstrated that incorporating the iCas9 gene in the B7-H3 CAR construct did not alter its effectiveness in recognizing and eliminating UM cells/tumors *in vitro* and *in vivo*.

Currently, a B7-H3-directed mAb targeting has demonstrated safety and potential clinical activity in the neoadjuvant setting in patients with localized prostate cancer in a single-arm phase 2 trial (19). Thus we compared the efficacy of our B7-H3 CAR T to an anti-B7-H3 mAb in a humanized mouse model. Our data show significant *in vitro* ability of NK cells to induce enhanced ADCC-mediated suppression of UM cell growth. However, anti-B7-H3 mAbs could only partially control tumor growth in humanized mice in contrast to iCas9.B7-H3 CAR T cells, which eradicated UM liver metastases in the same humanized mouse model. These findings raise the possibility that UM tumors may have greater intrinsic sensitivity to CAR T cells than ADCC, or discrepancies in TA binding affinity between our B7-H3 CAR construct, which is specific for the 376.96 B7-H3 epitope, and the utilized anti-B7-H3 mAb, which recognizes different B7-H3 epitopes. These discrepancies could be explained by intrinsic differences between mAb-based and cellular immunotherapies. As NK cells are weakly represented in

peripheral blood and the tumor microenvironment, and ADCC as an effector mechanism relies on multiple administrations of mAbs with a relatively short half-life, this may explain discrepancies in their ability to mount sustained antitumor activity. In contrast, CAR T cells have the advantage of *in vivo* expansion upon their transfer and long-term persistence if a memory pool is established (46).

Further in-depth mechanistic studies investigating the effects of the immunosuppressive systemic and local tumor microenvironment on the CAR T-cell–based immunotherapeutic strategy we have designed are limited by the lack of a syngeneic UM murine model. The lack of CAR T-cell generation from T cells derived from PBMCs derived from patients with cancer, which we have previously shown to be associated with a dysfunctional status, unfavorable memory phenotype, and reduced effector function as well as persistence of transferred T cells (38), may account for potential discrepancies between mouse studies and future clinical trials. In our *in vivo* experiments testing iCas9.B7-H3 CAR T cells in a model of high tumor burden, potent *in vivo* expansion was likely essential for the strong response of UM liver metastases to CAR T cells. However, CAR T cells generated by dysfunctional T cells from cancer patients or patients with high levels of circulating myeloid-derived suppressor cells may not sufficiently expand and achieve comparable results (32–34). These considerations provide the rationale to further explore CAR T cells with combinatorial strategies in patients with extensive tumor burden (40). Previous preclinical and clinical studies highlighted the efficacy of targeted therapies (MEK/HDAC, c-MET, and PKC inhibitors) targeting downstream pathways associated with driver mutations in the GNAQ and GNA11 genes (47, 48). These approaches demonstrate the potential to debulk UM liver metastases but not completely eradicate them, providing an opportunity for combinatorial strategies with CAR T cells in advanced, challenging-to-treat UM metastases. Tumor preconditioning with radiotherapy alone or in combination with disulfiram/copper, may mitigate other limitations such as B7-H3 downregulation, while boosting CAR T-cell stemness and their effector function (35, 38, 40).

In conclusion, iCas9.B7-H3 CAR T cells should be considered as a novel therapeutic strategy for patients with refractory metastatic UM and their use should be further investigated in other solid tumors with limited tumor immunogenicity.

Authors' Disclosures

G.M. Boland reports grants from Olink Proteomics, Teiko Bio, InterVenn Biosciences, and Palleon Pharmaceuticals as well as personal fees from Iovance, Merck, Nektar Therapeutics, Novartis, Ankyra Therapeutics, and InterVenn Biosciences and personal fees from Ankyra Therapeutics outside the submitted work. R.W. Jenkins reports personal fees from Xsphera Biosciences, G1 Therapeutics, Incyte, and Bioxcel Therapeutics outside the submitted work; in addition, R.W. Jenkins has a patent for US20200399573A9 licensed to Xsphera and a patent for US20210363595A1 licensed to Xsphera. X. Wang reports a patent for US10519214B2. S. Ryeom reports grants from Immpact Bio outside the submitted work. C.R. Ferrone reports a patent for US10519214B2. No disclosures were reported by the other authors.

Authors' Contributions

M. Ventin: Conceptualization, data curation, formal analysis, investigation, visualization, methodology, writing–original draft, writing–review and editing. **G. Cattaneo:** Conceptualization, data curation, formal analysis, investigation, visualization, methodology, writing–original draft, writing–review and editing. **S. Arya:** Formal analysis, investigation, methodology. **J. Jia:** Data curation, formal analysis, investigation, visualization, methodology. **M.C. Gelmi:** Data curation, formal analysis, funding acquisition, validation, investigation, visualization. **Y. Sun:** Data curation, formal analysis, investigation, visualization, methodology. **L. Maggs:** Formal analysis, investigation, visualization, methodology, writing–review and editing. **B.R. Ksander:** Resources, supervision, writing–review and editing. **R.M. Verdijk:** Resources, formal analysis, supervision, validation, methodology, writing–review and editing. **G.M. Boland:** Resources, supervision, writing–review and editing. **R.W. Jenkins:** Resources, formal analysis, supervision, funding acquisition, methodology, writing–review and editing. **R. Haq:** Resources, supervision, funding acquisition, validation, writing–review and editing. **M.J. Jager:** Resources, data curation, formal analysis, supervision, validation, writing–review and editing. **X. Wang:** Conceptualization, supervision, funding acquisition, methodology, project administration, writing–review and editing. **S. Ryeom:** Conceptualization, supervision, visualization, methodology, writing-original draft, project administration, writing–review and editing. **C.R. Ferrone:** Conceptualization, resources, supervision, funding acquisition, investigation, methodology, writing–original draft, project administration, writing–review and editing.

Acknowledgments

This article and significant contributions to immunology and CAR T-cell therapy are due to the landmark contributions of the late Dr. Soldano Ferrone, MD, PhD, who passed away in early 2023 at the age of 82 after an 8-week battle with COVID-19. Soldano Ferrone was a driving force in this multi-institutional collaborative effort. His absence is felt by family, friends, and colleagues, but his legacy and impact on us all continue to endure. We express our gratitude to Soldano Ferrone for his support in this work. We thank the Histopathology and Imaging CORE Facilities at the Massachusetts General Hospital and PARTS pathology research and trial service of the Erasmus MC for their assistance with tissue immunohistochemistry and animal imaging. This work was supported by the following funding sources: National Institutes of Health/National Cancer Institute R03CA280302 (C.R. Ferrone); National Institutes of Health/National Cancer Institute R01DE028172 (X. Wang); National Institutes of Health/National Cancer Institute R01CA226981 (X. Wang); National Institutes of Health/National Cancer Institute K08CA226391 (R.W. Jenkins); Department of Defense Idea Award W81XWH-20-PCRP-IDA (W81XWH2110433; X. Wang); Bontius Foundation (M.C. Gelmi); Oogfonds (M.C. Gelmi); SAM Fund (M.C. Gelmi); Leiden University Fund (LUF; M.C. Gelmi); P.A. Jager-van Gelder Fund (M.C. Gelmi); Blinden-Penning Foundation (M.C. Gelmi); Dawn K. Neher Fund for Ocular Melanoma Research (R. Haq); Pan-Massachusetts Challenge Team 3G (R. Haq); Massachusetts Life Sciences Center Research Infrastructure program funding for the MGH Tumor Cartography Center (R.W. Jenkins); and Massachusetts Life Sciences Center Research Infrastructure Program (R.W. Jenkins).

Note

Supplementary data for this article are available at Clinical Cancer Research Online (http://clincancerres.aacrjournals.org/).

Received January 8, 2024; revised March 5, 2024; accepted May 16, 2024; published first May 20, 2024.

References

1. Kaliki S, Shields CL. Uveal melanoma: relatively rare but deadly cancer. Eye (Lond) 2017;31:241–57.
2. Jager MJ, Shields CL, Cebulla CM, Abdel-Rahman MH, Grossniklaus HE, Stern MH, et al. Uveal melanoma. Nat Rev Dis Primers 2020;6:24.
3. Carvajal RD, Schwartz GK, Tezel T, Marr B, Francis JH, Nathan PD. Metastatic disease from uveal melanoma: treatment options and future prospects. Br J Ophthalmol 2017;101:38–44.
4. Chandran SS, Somerville RPT, Yang JC, Sherry RM, Klebanoff CA, Goff SL, et al. Treatment of metastatic uveal melanoma with adoptive transfer of tumour-infiltrating lymphocytes: a single-centre, two-stage, single-arm, phase 2 study. Lancet Oncol 2017;18:792–802.
5. Nathan P, Hassel JC, Rutkowski P, Baurain JF, Butler MO, Schlaak M, et al. Overall survival benefit with tebentafusp in metastatic uveal melanoma. N Engl J Med 2021;385:1196–206.
6. Carvajal RD, Butler MO, Shoushtari AN, Hassel JC, Ikeguchi A, Hernandez-Aya L, et al. Clinical and molecular response to tebentafusp in previously treated patients with metastatic uveal melanoma: a phase 2 trial. Nat Med 2022;28:2364–73.

7. Middleton MR, McAlpine C, Woodcock VK, Corrie P, Infante JR, Steven NM, et al. Tebentafusp, a TCR/anti-CD3 bispecific fusion protein targeting gp100, potently activated antitumor immune responses in patients with metastatic melanoma. Clin Cancer Res 2020;26:5869–78.
8. Rafiq S, Hackett CS, Brentjens RJ. Engineering strategies to overcome the current roadblocks in CAR T cell therapy. Nat Rev Clin Oncol 2020;17:147–67.
9. Park JH, Rivière I, Gonen M, Wang X, Sénéchal B, Curran KJ, et al. Long-term follow-up of CD19 CAR therapy in acute lymphoblastic leukemia. N Engl J Med 2018;378:449–59.
10. Locke FL, Ghobadi A, Jacobson CA, Miklos DB, Lekakis LJ, Oluwole OO, et al. Long-term safety and activity of axicabtagene ciloleucel in refractory large B-cell lymphoma (ZUMA-1): a single-arm, multicentre, phase 1 to 2 trial. Lancet Oncol 2019;20:31–42.
11. Shah NN, Lee DW, Yates B, Yuan CM, Shalabi H, Martin S, et al. Long-term follow-up of CD19-CAR T-cell therapy in children and young adults with B-ALL. J Clin Oncol 2021;39:1650–9.
12. Qi C, Gong J, Li J, Liu D, Qin Y, Ge S, et al. Claudin18.2-specific CAR T cells in gastrointestinal cancers: phase 1 trial interim results. Nat Med 2022;28:1189–98.
13. Del Bufalo F, De Angelis B, Caruana I, Del Baldo G, De Ioris MA, Serra A, et al. GD2-CART01 for relapsed or refractory high-risk neuroblastoma. N Engl J Med 2023;388:1284–95.
14. Hamid O, Sato T, Davar D, Callahan MK, Thistlethwaite F, Aljumaily R, et al. 728O results from phase I dose escalation of IMC-F106C, the first PRAME × CD3 ImmTAC bispecific protein in solid tumors. Ann Oncol 2022;33:S875.
15. Gelmi MC, Gezgin G, van der Velden PA, Luyten GPM, Luk SJ, Heemskerk MHM, et al. PRAME expression: a target for cancer immunotherapy and a prognostic factor in uveal melanoma. Invest Ophthalmol Vis Sci 2023;64:36.
16. Kontos F, Michelakos T, Kurokawa T, Sadagopan A, Schwab JH, Ferrone CR, et al. B7-H3: an attractive target for antibody-based immunotherapy. Clin Cancer Res 2021;27:1227–35.
17. Cattaneo G, Ventin M, Arya S, Kontos F, Michelakos T, Sekigami Y, et al. Interplay between B7-H3 and HLA class I in the clinical course of pancreatic ductal adenocarcinoma. Cancer Lett 2024;587:216713.
18. Du H, Hirabayashi K, Ahn S, Kren NP, Montgomery SA, Wang X, et al. Antitumor responses in the absence of toxicity in solid tumors by targeting B7-H3 via chimeric antigen receptor T cells. Cancer Cell 2019;35:221–37.e8.
19. Shenderov E, De Marzo AM, Lotan TL, Wang H, Chan S, Lim SJ, et al. Neoadjuvant enoblituzumab in localized prostate cancer: a single-arm, phase 2 trial. Nat Med 2023;29:888–97.
20. Chen Y, Zheng A, Zhang Y, Xiao M, Zhao Y, Wu X, et al. Dysregulation of B7 family and its association with tumor microenvironment in uveal melanoma. Front Immunol 2022;13:1026076.
21. Diaconu I, Ballard B, Zhang M, Chen Y, West J, Dotti G, et al. Inducible caspase-9 selectively modulates the toxicities of CD19-specific chimeric antigen receptor-modified T cells. Mol Ther 2017;25:580–92.
22. Foster MC, Savoldo B, Lau W, Rubinos C, Grover N, Armistead P, et al. Utility of a safety switch to abrogate CD19.CAR T-cell-associated neurotoxicity. Blood 2021;137:3306–9.
23. Jager MJ, Magner JAB, Ksander BR, Dubovy SR. Uveal melanoma cell lines: where do they come from? (An American Ophthalmological Society Thesis). Trans Am Ophthalmol Soc 2016;114:T5.
24. Versluis M, de Lange MJ, van Pelt SI, Ruivenkamp CAL, Kroes WGM, Cao J, et al. Digital PCR validates 8q dosage as prognostic tool in uveal melanoma. PLoS One 2015;10:e0116371.
25. Robertson AG, Shih J, Yau C, Gibb EA, Oba J, Mungall KL, et al. Integrative analysis identifies four molecular and clinical subsets in uveal melanoma. Cancer Cell 2017;32:204–20.e15.
26. Yang J, Tian Z, Gao H, Xiong F, Cao C, Yu J, et al. Clinical significance and correlation of PD-L1, B7-H3, B7-H4, and TILs in pancreatic cancer. BMC Cancer 2022;22:584.
27. Imai K, Wilson BS, Bigotti A, Natali PG, Ferrone S. A 94,000-dalton glycoprotein expressed by human melanoma and carcinoma cells. J Natl Cancer Inst 1982;68:761–9.
28. Jenkins RW, Aref AR, Lizotte PH, Ivanova E, Stinson S, Zhou CW, et al. Ex vivo profiling of PD-1 blockade using organotypic tumor spheroids. Cancer Discov 2018;8:196–215.
29. Daei Sorkhabi A, Mohamed Khosroshahi L, Sarkesh A, Mardi A, Aghebati-Maleki A, Aghebati-Maleki L, et al. The current landscape of CAR T-cell therapy for solid tumors: mechanisms, research progress, challenges, and counterstrategies. Front Immunol 2023;14:1113882.
30. Forsberg EMV, Lindberg MF, Jespersen H, Alsén S, Bagge RO, Donia M, et al. HER2 CAR-T cells eradicate uveal melanoma and T-cell therapy-resistant human melanoma in IL2 transgenic NOD/SCID IL2 receptor knockout mice. Cancer Res 2019;79:899–904.
31. Zhou T, Wang H-W. Antigen loss after targeted immunotherapy in hematological malignancies. Clin Lab Med 2021;41:341–57.
32. Locke FL, Rossi JM, Neelapu SS, Jacobson CA, Miklos DB, Ghobadi A, et al. Tumor burden, inflammation, and product attributes determine outcomes of axicabtagene ciloleucel in large B-cell lymphoma. Blood Adv 2020;4:4898–911.
33. Jain MD, Zhao H, Wang X, Atkins R, Menges M, Reid K, et al. Tumor interferon signaling and suppressive myeloid cells are associated with CAR T-cell failure in large B-cell lymphoma. Blood 2021;137:2621–33.
34. Ventin M, Cattaneo G, Maggs L, Arya S, Wang X, Ferrone CR. Implications of high tumor burden on chimeric antigen receptor T-cell immunotherapy: a review. JAMA Oncol 2024;10:115–21.
35. Wang T, Zhang K, You F, Ma R, Yang N, Tian S, et al. Preconditioning of radiotherapy enhances efficacy of B7-H3-CAR-T in treating solid tumor models. Life Sci 2023;331:122024.
36. Iaia I, Gammaitoni L, Cattaneo G, Giraudo L, Donini C, Fiorino E, et al. Recruitment, infiltration, and cytotoxicity of HLA-independent killer lymphocytes in three-dimensional melanoma models. Cancers (Basel) 2021;13:2302.
37. Giraudo L, Cattaneo G, Gammaitoni L, Iaia I, Donini C, Massa A, et al. CSPG4 CAR-redirected Cytokine Induced Killer lymphocytes (CIK) as effective cellular immunotherapy for HLA class I defective melanoma. J Exp Clin Cancer Res 2023;42:310.
38. Wang Y, Drum DL, Sun R, Zhang Y, Chen F, Sun F, et al. Stressed target cancer cells drive nongenetic reprogramming of CAR T cells and solid tumor microenvironment. Nat Commun 2023;14:5727.
39. Zhang Y, He L, Sadagopan A, Ma T, Dotti G, Wang Y, et al. Targeting radiation-resistant prostate cancer stem cells by B7-H3 CAR T cells. Mol Cancer Ther 2021;20:577–88.
40. Ventin M, Cattaneo G, Maggs L, Jia J, Arya S, Ferrone S, et al. B7-H3-targeted CAR T cell activity is enhanced by radiotherapy in solid cancers. Front Oncol 2023;13:1193963.
41. Dean EA, Mhaskar RS, Lu H, Mousa MS, Krivenko GS, Lazaryan A, et al. High metabolic tumor volume is associated with decreased efficacy of axicabtagene ciloleucel in large B-cell lymphoma. Blood Adv 2020;4:3268–76.
42. Hung HC, Fan MH, Wang D, Miao CH, Su P, Liu CL. Effect of chimeric antigen receptor T cells against protease-activated receptor 1 for treating pancreatic cancer. BMC Med 2023;21:338.
43. Stüber T, Monjezi R, Wallstabe L, Kühnemundt J, Nietzer SL, Dandekar G, et al. Inhibition of TGF-β-receptor signaling augments the antitumor function of ROR1-specific CAR T-cells against triple-negative breast cancer. J Immunother Cancer 2020;8:e000676.
44. Li M, Xue S-L, Tang X, Xu J, Chen S, Han Y, et al. The differential effects of tumor burdens on predicting the net benefits of ssCART-19 cell treatment on r/r B-ALL patients. Sci Rep 2022;12:378.
45. Norelli M, Camisa B, Barbiera G, Falcone L, Purevdorj A, Genua M, et al. Monocyte-derived IL-1 and IL-6 are differentially required for cytokine-release syndrome and neurotoxicity due to CAR T cells. Nat Med 2018;24:739–48.
46. Caruana I, Diaconu I, Dotti G. From monoclonal antibodies to chimeric antigen receptors for the treatment of human malignancies. Semin Oncol 2014;41:661–6.
47. Faião-Flores F, Emmons MF, Durante MA, Kinose F, Saha B, Fang B, et al. HDAC inhibition enhances the *in vivo* efficacy of MEK inhibitor therapy in uveal melanoma. Clin Cancer Res 2019;25:5686–701.
48. Rodrigues A, Cosman R, Joshua AM. LXS196 for metastatic uveal melanoma—finally some progress. Br J Cancer 2023;128:1791–3.